Article

Post-Weld Heat Treatment of S690QL1 Steel Welded Joints: Influence on Microstructure, Mechanical Properties and Residual Stress

Damir Tomerlin [1,*], Dejan Marić [2], Dražan Kozak [2] and Ivan Samardžić [2]

[1] R&D Department, DOK-ING Ltd., Slavonska Avenija 22G, 10000 Zagreb, Croatia
[2] Mechanical Engineering Faculty in Slavonski Brod, University of Slavonski Brod, Trg I. B. Mažuranić 2, 35000 Slavonski Brod, Croatia; dmaric@unisb.hr (D.M.); dkozak@unisb.hr (D.K.); ivan.samardzic@unisb.hr (I.S.)
* Correspondence: damir.tomerlin@dok-ing.hr or damirtomerlin@gmail.com

Abstract: During the manufacturing of welded structures, some degree of residual stresses occurs. The classic approach to residual stress reduction is Post-Weld Heat Treatment (PWHT). In the case of structural grade mild steels, the thermal process is well established. In case of S690QL1 High Strength Steel (HSS), which is manufactured using the Quenching and Tempering (QT) process considered in this paper, only limited PWHT treatment is possible without deterioration of mechanical properties. Since this steel grade is susceptible to subsequent heat input, the challenge is to establish adequate PWHT parameters, achieving residual stress reduction while retaining sufficiently high mechanical properties. The paper considers X joint welded HSS steel plates with slightly overmatching filler metal. The welded coupon is prepared and subjected to PWHT treatment. The research on the influence of heat treatment was performed using the four different PWHT cycles and initial As-Welded (AW) material condition. The authors proposed those PWHT cycles based on available resources and the literature. Process holding temperature is considered the variable parameter directly related to the behaviors of material properties. The methodology of welded joint analysis includes experimental testing of mechanical properties, metallographic examination, and residual stress quantification. Testing of mechanical properties includes tensile testing, Charpy V-notch impact testing, and hardness testing in scope of complete welded joint (BM + HAZ + WM). Metallographic examination is performed in order to characterize the welded joint material in relation to applied PWHT cycles. In order to quantify residual stresses, all heat-treated samples were examined via the X-ray diffraction method. Mechanical properties testing determined that an increase in PWHT cycle holding temperature leads to degradation of tested mechanical properties. For specific zones of the welded joint, the decreasing trend from AW condition to Cycle D (max. 600 °C) can be quantified. Based on representative specimens comparison, strength values (BM ≤ 5.7%, WM ≤ 12.1%, HAZ ≤ 20%), impact testing absorbed energy (BM = 17.1%, WM = 25.8%, FL = 12.5%, HAZ = 0.6%), and hardness values (BM = 4.1%, WM = 3.2%, CGHAZ = 16.6%, HAZ = 24.2%) are all exhibiting decrease. Metallographic examination, using the light microscopy, after the exposure to PWHT thermal cycles, did not reveal significant changes in the material throughout all specific welded joint segments. Average relative reduction in residual stress in correlation with PWHT temperature can be observed (AW = 0%, Cycle A (max. 400 °C) = 72%, Cycle B (max. 530 °C) = 81%, Cycle C (max. 550 °C) = 93% and Cycle D (max. 600 °C) = 100% stress reduction). It can be concluded that S690QL1 HSS welded joints can generally be subjected to PWHT, while adhering to the limits of the material and process. In the authors' shared opinion, it is advisable to use the PWHT Cycle C (max. 550 °C) with 93% RS reduction, while mechanical properties retain high values.

Keywords: welded joint; high strength steel; Post-Weld Heat Treatment; metallographic examination; mechanical properties; residual stress

1. Introduction

High demands on modern welded structures, such as vehicle chassis, refer to exceptional load-bearing capacity while retaining the principles of lightweight design. Good weldability and machinability are also mandatory [1–4]. Conventional structural steels can only partially fulfill such requirements. The high-strength structural steels are, therefore, imposed as a viable solution. There are several categories of high-strength steels available, such as High Strength Low Alloy (HSLA), High Yield (HY), Quenched and Tempered (QT), and Thermo-mechanically Controlled Process (TMCP) steels [5–8]. This paper focuses only on QT high-strength steel, which is covered in detail.

The high mechanical properties of QT steel, which are related to strength and toughness, are achieved via selective alloying and special manufacturing process. Prerequisites for high toughness are controlled low contents of phosphorus and sulphur. The required alloy content is exactly adjusted to ensure an optimum combination of mechanical properties and good machinability. Following the increase in plate thickness, the content of alloying elements is also increased to ensure the required mechanical properties after quenching and tempering. Good weldability is ensured through maintaining the low carbon equivalent CEV and CET values.

The QT steel manufacturing process includes rolling in order to achieve sufficient deformation in the core of the plate. The rolling process parameters, including temperature, force, and thickness reduction ratio, must be carefully monitored during production. Such rolled microstructure is optimally suited to subsequent quenching and tempering. Thermal treatment includes heating up to the austenitizing temperature, followed by rapid cooling. Rapid cooling water quenching process enables the formation of a fine-grained, hard microstructure. The subsequent tempering leads to material softening and the start of precipitation processes, resulting in a final microstructure, which is composed of martensite and tempered troostite or bainite, with high strength and good toughness [3,4,9–13].

QT HSS steels generally gain good weldability through the fusion welding processes, while also adhering to the specific process guidelines. Welding should be carried out according to controlled technological procedures, with established filler metals, pre-heating, heat input, and cooling time $t_{8/5}$ parameters, as well as PWHT in cases where applicable. Following the increase in the strength of steel, the permissible limits of welding heat input are drastically reduced; thus, the welding process must be under strict control [3,4]. HSS can be readily welded using various filler metals. For HSS of very high strength values ($R_{p0.2} \geq 1000$ MPa), there are currently no suitable strength-matching filler metals available; thus, it is necessary to make welded joints of undermatching quality.

Welding process is accompanied by dissimilar thermal expansion and contraction of welded joint molten zone i.e., the weld and base metal. Cooling of weld metal causes its contraction, which in turn causes the occurrence of tensile residual stress (RS), which is particularly dominant in the longitudinal direction. Transverse residual stresses also occurs during those thermal changes. Aside from residual stresses, problems of excessive distortions and buckling of overall structures often appears, which is especially pronounced in thin-walled structures. In contrast, welded thick plates experience a more pronounced influence from residual stresses. Residual stress levels in the Weld Metal (WM), Heat Affected Zone (HAZ), and Adjacent Base Metal (BM) can reach very high values, which, in highly constrained structures, can even equal the material yield strength [14,15].

High-tensile residual stresses are an extremely unfavorable phenomenon in engineering structures, since, in static loading conditions, they reduce the permissible external load on welded joints. The impact on fatigue is also significant, since the externally applied fluctuating stresses are superimposed onto the internal residual stress. This issue becomes very relevant for dynamically loaded welded structures, e.g., military and construction vehicles. Theoretical investigation into the residual stress distribution in steel plates welded either at the center or at the edge was discussed by Tall [15].

The HSS steel-welded structures, during their exploitation period, are subjected to different types of loads and conditions. They are, thus, susceptible to several failure modes:

stress corrosion cracking (SCC), fatigue-induced damage, and Hydrogen-Induced Cracking (HIC); all of these problems are strongly dependent on the material microstructure and welding residual stress [16]. Reducing the tensile residual stresses helps to establish the dimensional control, improve fracture performance, and prevent some forms of cracking, while improving structures' overall resistance to failure. A number of publications deal with the influence of residual stress on high-strength steel. Influence of RS on HSLA steel welds was investigated by Alipooramirabad et al. [16], while the fatigue life of S700MC steel welds was investigated by Bukovská et al. [17].

Welding-induced residual stresses can be relieved via thermally activated processes, specifically Post-Weld Heat Treatment (PWHT). This is a time–temperature-related phenomenon where, instead of short time periods at high-temperature exposure, similar stress relief level can be obtained via holding a component for longer periods at a lower temperature. Material stress relaxation behavior is characterized via microscopic creep at the temperature of stress relief. PWHT is generally related to annealing treatment in a temperature area below A_1 [18,19].

Investigations into PWHT influence on residual stresses, microstructure, and mechanical properties were previously performed for different HSS steel grades by various researchers. High-temperature PWHT effects on Quenched and Tempered (QT) Bisalloy 80 steel welds were investigated by Alipooramirabad et al. [20]. A significant reduction in residual stress took place, which was combined with hardness drop and microstructural changes throughout the welded joint zones. Post-weld heat treatment of S690 high-strength steel welded connections was performed by Zhao et al. [21]. Hole drilling tests reveal that PWHT is able to reduce residual stress levels, while tensile testing shows improvement in the ductility and the maximum resistance. Overheating can severely reduce the load-carrying capacity. Experimental investigation and numerical simulations of annealing temperature influence on residual stresses in S700MC steel welds were performed by Kik et al. [22], showing that the increase in the annealing temperature in each analyzed case caused a decrease in the level of residual stresses. PWHT effect on microstructure and fracture toughness of X80 pipeline steel-welded joint was investigated by Wang et al. [23].

Even though thermal relaxation of residual stresses is most commonly employed method, there are several mechanical methods for relieving peak stresses or their redistribution. Those methods are as follows: overloading, vibration, peening or shot blasting, grinding, and explosion relaxation [19]. The High-Frequency Mechanical Impact (HFMI) treatment of S690QL steel welded joints for residual stress relaxation was performed by Ono et al. [24]. The Vibratory Stress Relief (VSR) method, as an alternative to heat treatment, uses controlled vibrations to cause external dynamic loading on residual stresses internal load, introducing plasticity into materials [25,26].

This paper and its related investigation aims to determine the influence of various PWHT treatments on welded joints made from S690QL1 High Strength Steel (HSS). Since this steel grade is susceptible to heat input, the challenge is to establish optimal PWHT parameters, achieving the satisfactory level of residual stress reduction, while also retaining sufficiently high mechanical properties. In this paper, the X-welded joint is described and several PWHT Cycles are proposed. Experimental investigation covers mechanical properties [27,28], metallographic examination, and residual stress measurements. The conclusions of the investigations performed are provided in the final section.

2. Materials and Methods

The high-strength steel investigated in this paper was S690QL1 grade. It is a fine-grained structural steel of high yield strength manufactured via the Quenching and Tempering (QT) process, with hot rolled products supplied according to EN 10025-6 standard. According to standard classification, this steel grade has the guaranteed yield strength $R_{p0.2} \geq 690$ MPa, while tensile strength is in the range R_m = 770–940 MPa, which is valid for plate thickness up to 50 mm. QL1 corresponds to extra-tough grade with minimum notch toughness values determined at -60 °C [9,10].

Considering the high mechanical properties of steel, which were required due to the high exploitation loads of the welded joints, the corresponding high strength Mn3Ni1CrMo (ER110S-G) filler metal was used [11]. The filler declared yield strength was $R_{p0.2} \approx 800$ MPa, which indicated the slightly Over-Matching (OM) weld metal. Base Steel Material (BM) and Filler Weld Metal (WM) mechanical properties and chemical composition, as provided in manufacturer certificates, are given in Tables 1 and 2.

Table 1. Mechanical properties of S690QL1 and Mn3Ni1CrMo [9–11].

Material	$R_{p0.2}$	R_m	A_5	ISO-V [2]
	[MPa]	[MPa]	[%]	[J]
S690QL1 [1]	787	841	22	108 (−60 °C)
Mn3Ni1CrMo	800	900	19	190 (20 °C)

$R_{p0.2}$: yield strength; R_m: tensile strength; A_5: percentage elongation after fracture; ISO-V: Charpy V-notch impact strength. [1] valid for 40 mm plate thickness, [2] transverse oriented specimen.

Table 2. Chemical composition of S690QL1 and Mn3Ni1CrMo [9–11].

Material	C	Si	Mn	Ni	Cr	Mo	Cu	Al	V	P	S	CEV [1]	CET [2]
	Chemical Element [% by Weight]												
S690QL1	0.17	0.25	1.20	0.05	0.33	0.21	0.03	0.075	0.01	0.011	0.001	0.49	0.33
Mn3Ni1CrMo	0.10	0.53	1.60	1.40	0.32	0.269	0.02	0.005	0.075	0.012	0.006	0.59	0.34

[1] CEV = C + Mn/6 + (Cr + Mo + V)/5 + (Cu + Ni)/15—carbon equivalent according to International Institute of Welding (i.e., CE_{IIW}); [2] CET = C + (Mn + Mo)/10 + (Cr + Cu)/20 + Ni/40—carbon equivalent according to EN 1011-2.

The welded test coupon was made from 40 mm thick steel plates, which were joined with double V-butt weld (X-welded joint). The overall test coupon length was 1000 mm, which was needed to accommodate all the test specimens. Groove preparation was previously performed via machining according to recommendations given in EN ISO 9692-1, for joint Ref. No. 2.5.1 (Figure 1a). Weld metal was deposited, in multi-pass configuration, using the Gas Metal Arc Welding (GMAW) process with 1.2mm diameter filler wire (Figure 1b).
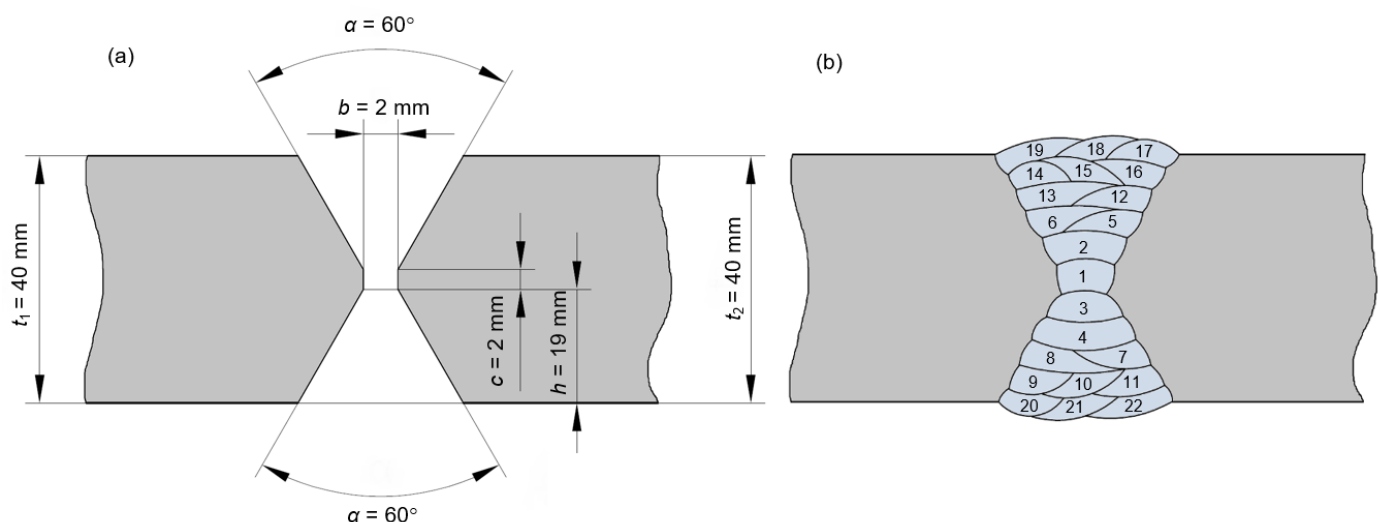

Figure 1. X-welded joint: (**a**) joint groove geometry and preparation; (**b**) welding passes.

Considering the 40mm BM material thickness and the joint groove preparation, a total of 22 welding passes were required to produce the X weld. Welding was performed in ISO 6947: PA (1G) plate flat position. Alternating welding between the upper and lower welded joint grooves was applied. In this way, control of heat input was achieved, and distortion

of the plates and the complete welded joint was prevented. Pre-heating was performed according to HSS requirements, using the oxyacetylene flame reaching a temperature of $T_p \leq 100\ °C$. The interpass temperature was limited to $T_i \leq 180\ °C$. The shielding gas used was M21 82% Ar + 18% CO_2 mixture, with a flow rate of 12–16 L/min. The process parameters selected considered the special requirements of steel base metal, filler metal, and welded joint geometry. These parameters are listed in Table 3.

Table 3. Welding process parameters.

Pass No.	Location	I	U	v_w	η	Q
		[A]	[V]	[cm/min]		[kJ/mm]
1–3	root	195	26	28.5	0.8	0.85
4–22	fill + cover	280	29	45	0.8	0.87

After the completion of the welding process, the welded test coupon was subjected to an elaborate NDT inspection. The welded joint surface was inspected using the magnetic particle testing (MT) method according to ISO 17,638 and visual inspection (VT) according to ISO 17637. No linear indications were detected. Volumetric inspection of welded joint material was performed using the radiographic testing (RT) method according to ISO 17636-1; it did not detect any internal defects (Figure 2).

Figure 2. X-welded joint radiographic testing (RT) according to ISO 17636-1.

The inspected welded test coupon was then prepared and marked for specimen subsections extraction and subsequent PWHT cycles treatment (Figure 3).

Specimen subsections of cuboid shape, which were divided into groups and enumerated from 1 to 9 according to specific testing procedures, were separated mechanically from the test coupon using a band saw. Further subsections division was performed according to 4 different PWHT cycles (marked with letters A to D) and initial As-Welded (AW) material condition (marked with letter E) (Figure 4).

The specific testing procedures according to specimen groups are as follows (Figure 3):

- 1—Tensile testing (BM), L direction
- 2—Impact Charpy V-notch testing (BM), T-L direction
- 3—Additional testing (SEM, EDS analysis, etc.)—not in scope of this paper
- 4—Tensile testing (BM), T direction
- 5—Tensile testing (WM + HAZ), L direction
- 6—Macro, micro, hardness, and residual stress (RS) testing, T direction
- 7—Impact Charpy V-notch testing (WM—center), T-L direction
- 8—Impact Charpy V-notch testing (FL—fusion line), T-L direction
- 9—Impact Charpy V-notch testing (HAZ), T-L direction

The specimen orientation was determined with L for the longitudinal direction corresponding to the plates' Rolling Direction (RD) and Welding Direction (WD). Transverse direction was determined with letter T, while T-L denotes transverse-oriented specimen with a notch in longitudinal direction.
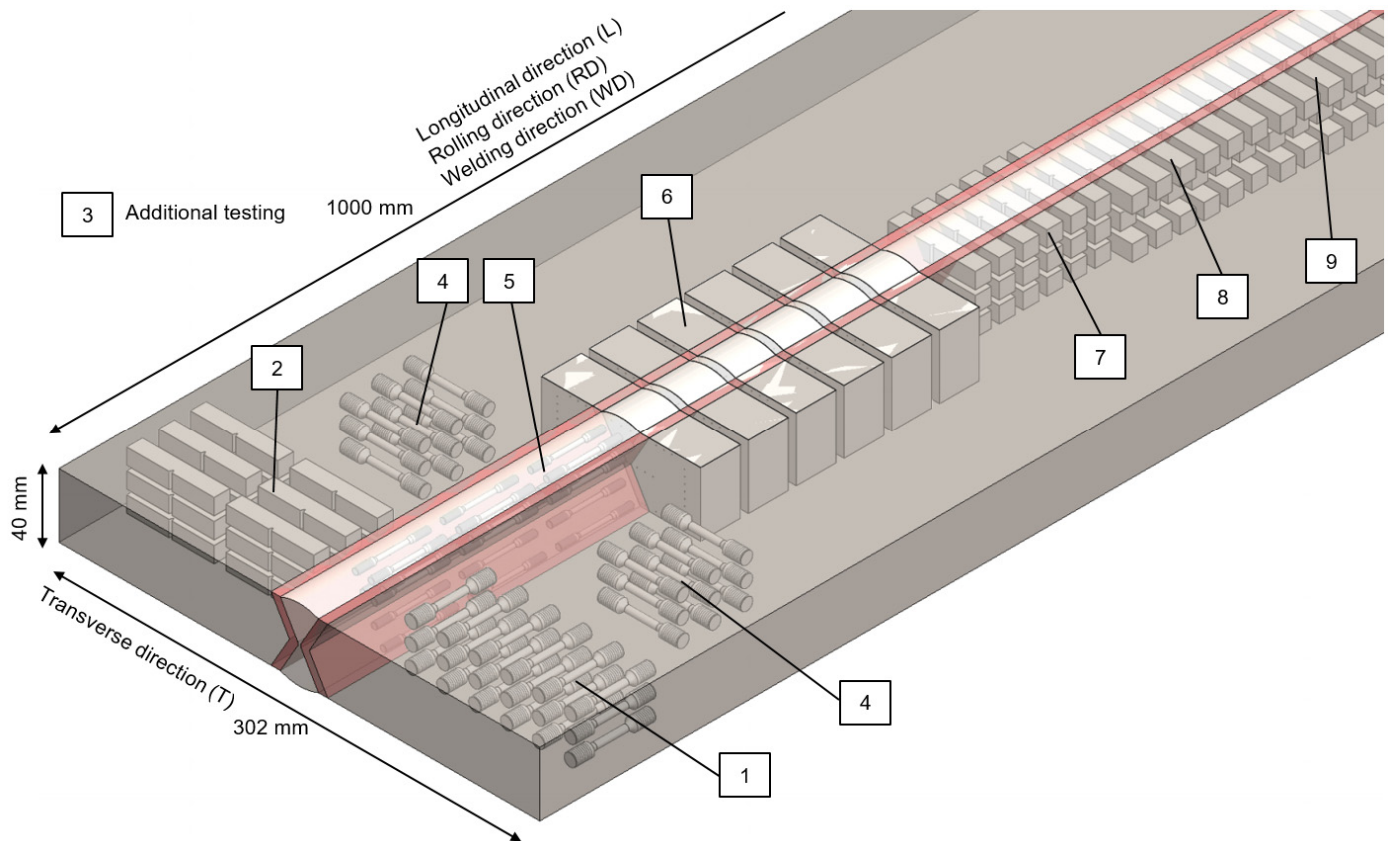
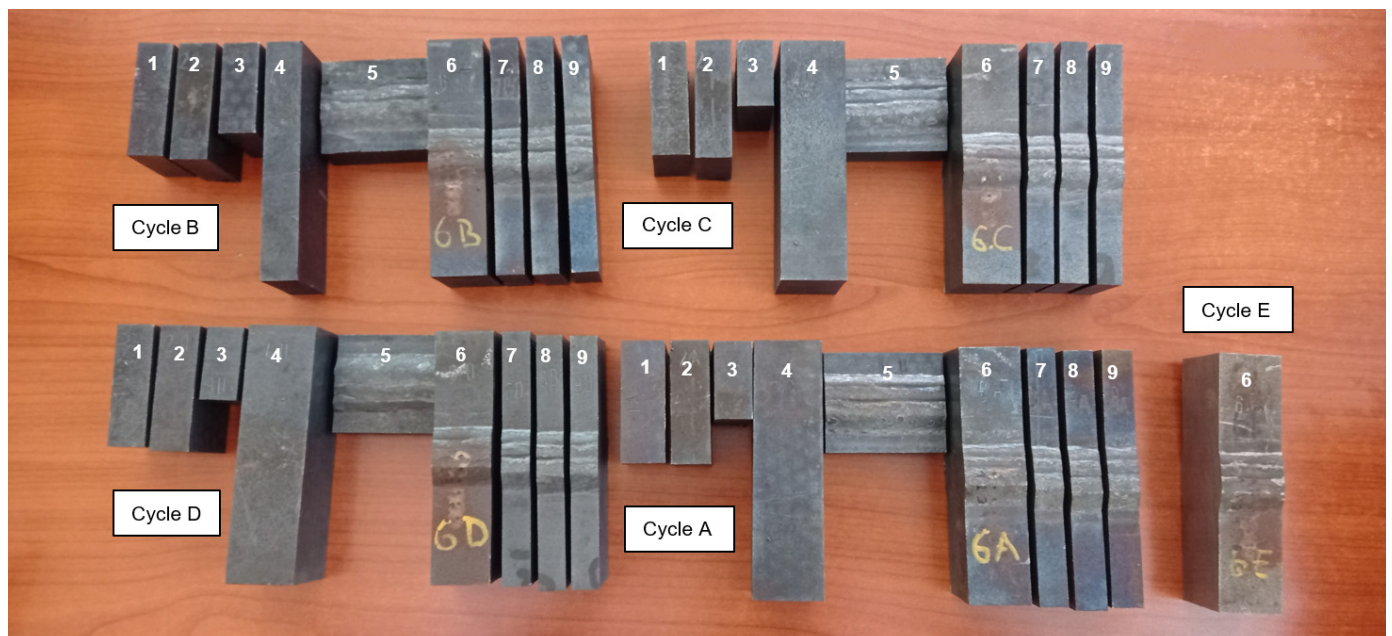**Figure 3.** Welded test coupon with disposition of test specimens.

Figure 4. Specimen subsections sorted according to PWHT cycles and test procedures.

The influence of Post-Weld Heat Treatment (PWHT) on steel material properties and residual stress reduction was determined using the 4 different PWHT cycles, and results were compared with the initial As-Welded (AW) material condition. Since fine-grained QT HSS steel in general is susceptible to external heat influence, the highest heat treatment temperatures should be maintained at 30–40 °C below the tempering temper-

ature of the steel-quenching process. According to manufacturer recommendations, the stress relief annealing for constructional reasons should be performed in the temperature range 530–580 °C [4]. ASM heat treatment defines similar temperature ranges and relationships between temperature, holding time, and residual stress relief [18]. The conservative approach was defined in AWS D1.1/D1.1M structural welding code for steel standard, advising against PWHT of QT steels weldments, specifically ASTM A709-100 grade corresponding to S690QL1 HSS. Taking into account the available information from the existing literature and their own predictions, the authors defined all the parameters of PWHT cycles, as given in Table 4.

Table 4. Thermal periods and parameters of Post-Weld Heat Treatment (PWHT) cycles.

Cycle	Thermal Period	Time	Temperature	Rate of Heating/Cooling
		[h]	[°C]	[°C/h]
A (max. 400 °C)	Pre-heating	2	20 → 150	65
	Warming	2	150	0
	Heating	3.5–4.5	150 → 400	+(55–75)
	Holding	4	400	0
	Cooling in furnace	1–1.5	400 → 315	−(55–80)
	Cooling in air	≥3	315 → 20	still air
B (max. 530 °C)	Pre-heating	2	20 → 150	65
	Warming	2	150	0
	Heating	5–7	150 → 530	+(55–75)
	Holding	4	530	0
	Cooling in furnace	2.5–4	530 → 315	−(55–80)
	Cooling in air	≥3	315 → 20	still air
C (max. 550 °C)	Pre-heating	2	20 → 150	65
	Warming	2	150	0
	Heating	5–7.5	150 → 550	+(55–75)
	Holding	4	550	0
	Cooling in furnace	3–4.5	550 → 315	−(55–80)
	Cooling in air	≥3	315 → 20	still air
D (max. 600 °C)	Pre-heating	2	20 → 150	65
	Warming	2	150	0
	Heating	6–8	150 → 600	+(55–75)
	Holding	4	600	0
	Cooling in furnace	3.5–5	600 → 315	−(55–80)
	Cooling in air	≥3	315 → 20	still air
E	As-Welded (AW)	-	-	-

Cycle A: low-temperature cycle; Cycle B: minimum recommended stress-relieving temperature for S690QL1 grade; Cycle C: mid-range stress- relieving temperature for S690QL1 grade; Cycle D: maximum recommended stress-relieving temperature for S690QL1 grade; Cycle E: As-Welded (AW) condition.

PWHT treatment of specimen subsections was performed in industrial furnace with protective atmosphere and internal temperature monitoring. The influence of heat treatment on color change in samples A to D in relation to As-Welded sample E was indicative (Figure 4).

Thermal cycles were defined with certain characteristic periods. Pre-heating to 150 °C during the 2 h period, followed by a warming period (holding at 150 °C for 2 h), is characteristic of all cycles. This process was carried out for the purpose of low-temperature relaxation of possible quenched areas in the weld and HAZ regions, achieving uniform temperature throughout the entire volume of a structure and reducing the risk of thermal stresses and deformation in continuation of PWHT process. Heating from 150 °C to holding temperature, dependent on the specific cycle, was carried out with regulated heating rate from 55 °C/h to 75 °C/h. This heating rate was determined with regard to thick welded plates (40 mm to 80 mm) in order to prevent temperature differences throughout

structure being greater than 140 °C, as well as preventing the occurrence of undesirable thermal deformations. At temperatures above 500 °C, the temperature difference between individual areas of the structure did not exceed 100 °C, as mandated by the ISO BS PD 5500 Specification for unfired fusion-welded pressure vessels. The holding temperatures and time were determined according to the recommendations for massive constructions made of high-strength steel with differences in the thickness of the welded elements. Holding temperatures from 550 to 575 °C reduced residual stresses by 80 to 90% compared to the AW condition [19]. Holding time was 4 h for all cycles, with this length being determined based on recommendations given in standards BS 1515, AWS D1.1/D1.1M, ASME BPVC, Section VIII, etc. To gain better insights into PWHT influence, holding time was also optimized for future investigations. Cooling was slow enough that no significant temperature differences and new thermal stresses occur in the annealed structure. Regulated cooling in furnace was performed at a temperature of 315 °C, with a cooling rate between 55 and 80 °C/h. Further cooling from 315 °C to room temperature was performed in still air, i.e., with the furnace door open. For better visualization and the possibility of mutual comparison, PWHT cycles with corresponding curves are shown in the graph form (Figure 5).
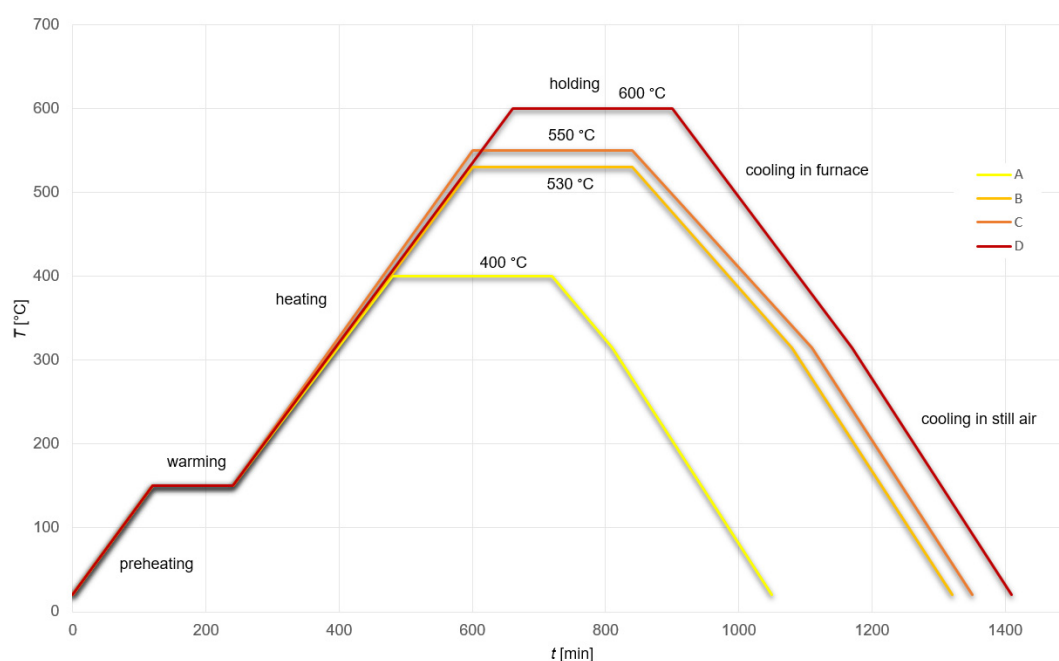

Figure 5. PWHT cycles graph with characteristic temperature, *T* [°C]—time, *t* [min] curves. Cycle A (max. 400 °C), Cycle B (max. 530 °C), Cycle C (max. 550 °C), and Cycle D (max. 600 °C).

It was observed that in each PWHT cycle, a variation in heating and cooling times, as well as holding temperature parameters, took place. Since heating and cooling times were directly dependent on holding temperature and their rate was maintained constant in all cycles, their influence on material properties was not separately studied. The authors focused on the process holding temperature as the individual variable parameter determining the mechanical properties and residual stresses.

Following the PWHT treatment, mechanical properties of specimens were tested, along with the macroscopic and microscopic observations. All the test procedures are listed (Figure 3). The corresponding equipment used is described in continuation.

Tensile testing of BM material in longitudinal (L) and transverse (T) directions (specimen groups 1 and 4) was performed according to ASTM E8 standard. Round tension test small-size proportional specimen, with specific dimensions: *D* = 4 mm, *L* = 50 mm, and *A* = 20 mm, and M8 threaded ends were machined and prepared. Tensile testing of WM and HAZ regions in L direction (specimen group 5) was also performed according to ASTM E8 standard. Since the investigated areas were of small material volume, round tensile

subsize specimens, with specific dimensions: D = 2.5 mm, L = 46 mm, and A = 20 mm, and M4 threaded ends were required. A total of 7 tensile specimens were placed in the specimen subsection: 3 specimens were allocated for WM and 4 specimens were allocated for HAZ testing. The subsection was first cut into 7 pieces, after which stage the tensile test specimens were machined and prepared (Figure 6). All mechanical tests were performed at ambient temperature, using Messphysik BETA 250 testing machine (Messphysik Materials Testing GmbH, Fürstenfeld, Österreich), (Figure 7).
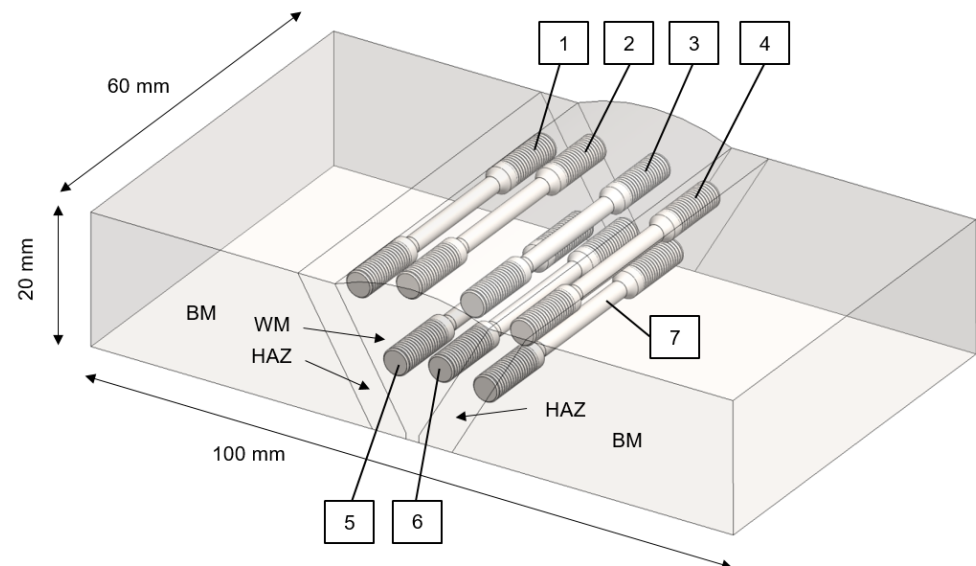

Figure 6. Tensile testing of WM and HAZ in L direction (specimen group 5): WM specimens: 2, 3, and 6; HAZ specimens: 1, 4, 5, and 7.
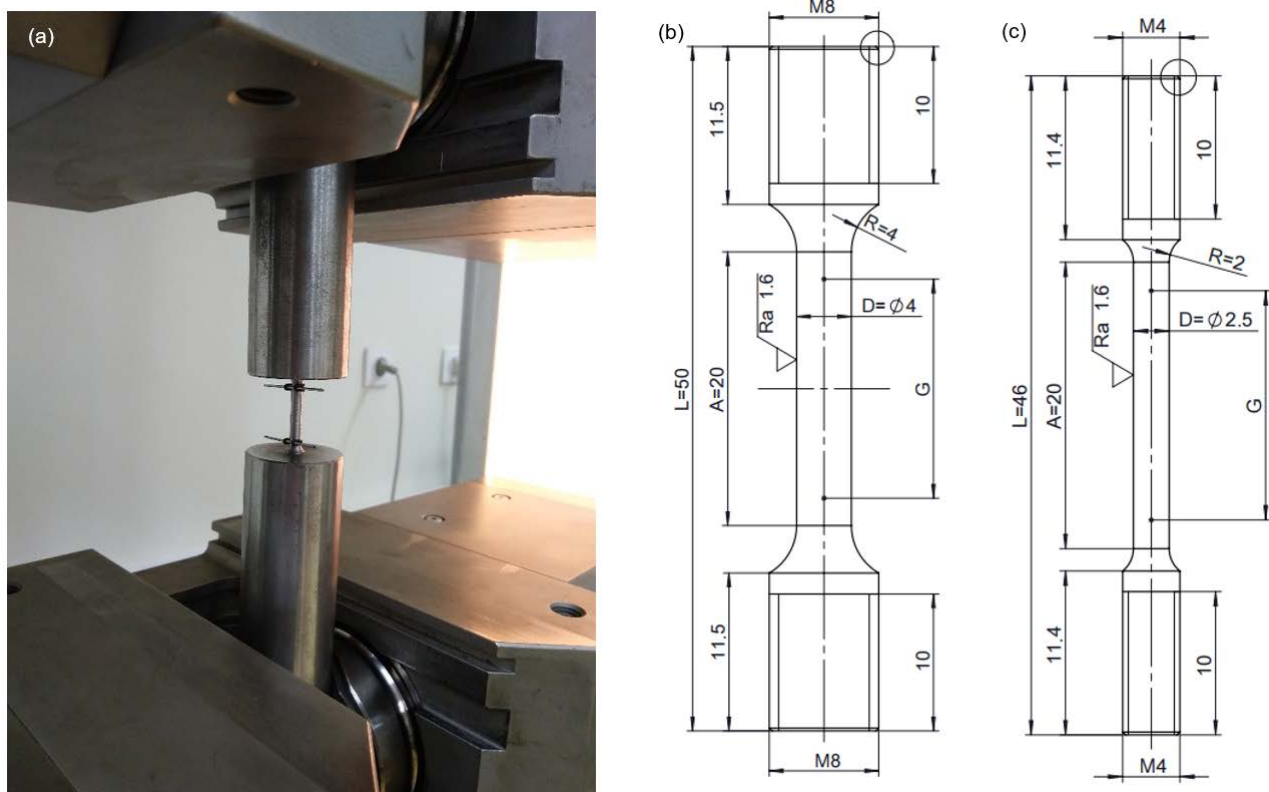

Figure 7. Tensile testing: (**a**) Messphysik BETA 250 testing machine; (**b**) ASTM E8 specimen D = 4 mm, M8 threaded ends; (**c**) ASTM E8 specimen D = 2.5 mm, M4 threaded ends.

Impact Charpy V-notch testing of BM material in transverse-longitudinal (T-L) direction (specimen group 2), and WM, FL, and HAZ (specimen groups 7, 8 and 9) was performed according to EN ISO 148-1 standard (Figure 8). Standard V-notch $10 \times 10 \times 55$ mm specimens were used. Testing was performed at an ambient temperature of +22 °C, using Zwick Roell RKP 450 Charpy pendulum impact testing machine (Zwick Roell Gruppe, Ulm, Germany) with 450 J pendulum head.
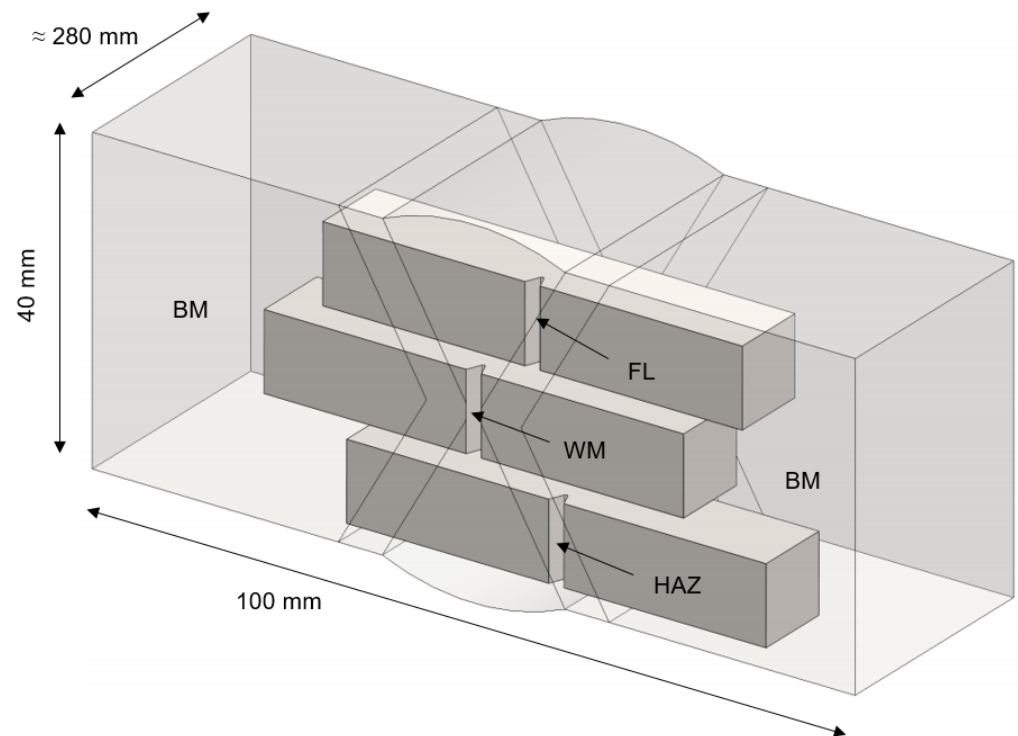

Figure 8. Impact Charpy V-notch testing of BM (specimen group 2) and WM, FL and HAZ (specimen groups 7–9) in T-L direction.

Macroscopic and microscopic observations of welded joints, covering BM, HAZ and WM zones of interest, were performed on extracted and specially prepared cross-sectional specimens (specimen group 6) according to ISO 17,639 standard, (Figure 9). Specimens had dimensions of $100 \times 40 \times 30$ mm, with the observed weld surface processed via polishing and etching using the 3% HNO_3 nitric acid in ethyl alcohol (Nital), according to ISO/TR 16,060 standard. Macroscopic observations were performed using Olympus SZX10 (Olympus Corporation, Tokyo, Japan) multifunctional stereoscopic microscope. Microstructural observations were performed using Zeiss Axioskop 2 MAT light microscope with magnifications in range of 50–1000 ×.

Hardness measurements were performed on the same samples previously used for macroscopic and microscopic observations (specimen group 6) according to the EN ISO 9015-1 standard for hardness test on arc-welded joints. The Vickers method HV 10 was used with an indenter test load of 98.07 N. Hardness distributions were measured along the lines 1–3, which corresponded to the top, centerline, and bottom regions of the X-welded joint (Figure 9). Universal hardness tester Zwick Roell ZHV-10 B3212 (Zwick Roell Gruppe, Ulm, Germany) was used.

Additional testing (specimen group 3) relates to Scanning Electron Microscopy (SEM), Energy-Dispersive Spectroscopy (EDS), and other analyses that were not performed in the scope of this work. The authors plan to conduct these analyses in future research on this topic.
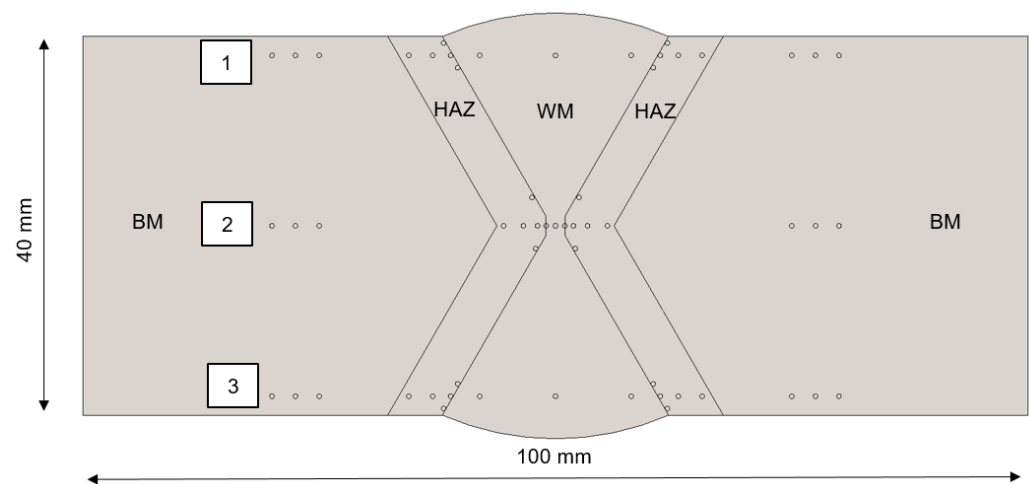
Figure 9. Macroscopic, microscopic, and hardness HV 10 testing of X-welded joint, including BM, WM, and HAZ regions (specimen group 6) in T direction.

In order to evaluate the influence of previously implemented PWHT on residual stress reduction, X-welded joints were subjected to experimental quantification of residual stress levels. Measurements were performed on the same transverse oriented specimens previously used for macro/micro observations and hardness testing (specimen group 6). The X-ray diffraction method [29–31] using the Xstress 3000 G2R (Stresstech Group, Jyväskylä, Finland) was used. The operation of the device was based on the diffraction of X-rays on the crystal lattice of the material using Bragg's law ($\lambda = 2d\sin\theta$), where the X-ray wavelength (λ) was known, the distance between atomic planes (d) was not known, and the diffractions were observed at angles (θ). Applied or residual stresses induced a strain corresponding to changes in crystal lattice spacing. The method measured elastic strain, which was consequently converted to stress using the Hooke's law principle, with elastic modulus (E) and Poisson's ratio (ν). XRD method included a thin surface layer of material (≤ 10 μm), measuring the near-surface residual stress. This method assumed the existence of only surface stresses (i.e., plane stress condition), with surface stresses σ_{11} and $\sigma_{22} \neq 0$ and stress normal to surface $\sigma_{33} = 0$.

Stress components σ_{11} corresponding to x longitudinal direction, and σ_{22} corresponding to *y* transverse direction, were measured. Measurements were taken on the top surface of welded specimens in a linear sequence of 6 points. Point 1 was located at the weld centerline. The distance between the points was 5 mm. Prior to measuring, all the points were prepared through electropolishing for 30 s. For all measurements, a chromium (CrKa) X-ray tube was used. The measuring method used was modified $d(\sin^2\psi)$. The *hkl* diffractive plane 211 and diffraction angle $\theta = 156.4°$ were used. For calculation of residual stresses using Hooke's law and elastic strain theory, the elastic modulus E = 210 MPa $\pm 5\%$ and Poisson's ratio $\nu = 0.3$ were taken. The experimental setup for X-ray diffraction (XRD) measurement of residual stresses using Stresstech Xstress 3000 G2R on X-welded joint specimen (group 6) is shown in Figure 10.
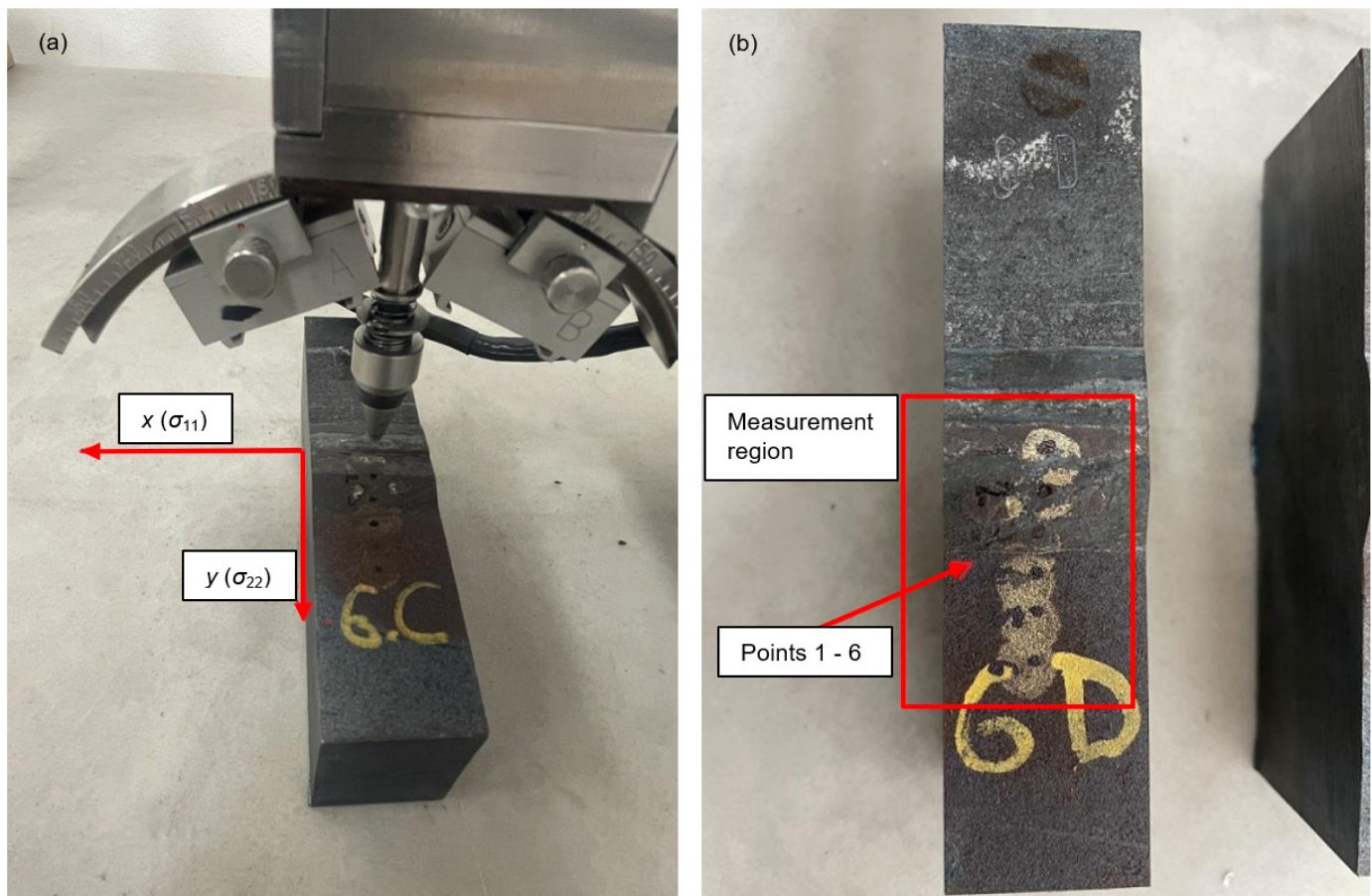
Figure 10. Residual stress experimental setup: (**a**) Stresstech Xstress 3000 G2R X-ray diffraction method residual stress analyzer with marked stress components σ_{11} and σ_{22}; (**b**) specimen with measuring points 1–6 on upper surface.

3. Results

The goal of the research carried out in the paper is to experimentally investigate the influence of different PWHT cycles on mechanical properties of welded joint materials and residual stress reduction. All the testing procedures are previously listed and shown (Figure 3), while the methodology and equipment used are described in detail. Results of testing procedures are given in the continuation, where they are separated and structured into three major subsections: mechanical testing, metallographic examination, and residual stress.

3.1. Mechanical Testing

3.1.1. Tensile Testing

In scope of the tensile testing, the following characteristic values of the material are determined for each tensile specimen: yield strength ($R_{p0.2}$), tensile strength (R_m), percentage elongation after fracture (A_5), and Young's modulus (E). Corresponding stress–strain (σ–ε) curves are also experimentally obtained. In accordance with the expectations of the examination, four different PWHT cycles (marked A to D) and initial As-Welded (AW) material condition (marked E) are subjected to a tensile test. Initially, the general behavior of the base HSS steel metal S690QL1 is determined. For each PWHT material condition, three tensile specimens are tested to gain an additional level of confidence. Tensile testing is performed in L—longitudinal direction, with results given in Table 5, as well as in T—transverse direction, with results given in Table 6. Strength testing of BM in condition after welding (AW) determined the average yield strength as $R_{p0.2}$ = 736.6 MPa, and average

tensile strength as R_m = 810.3 MPa values, measured in L direction. In the T direction, the average yield strength of $R_{p0.2}$ = 771.7 MPa, and average tensile strength of R_m = 837.3 MPa, are determined. These values fit well in the yield strength $R_{p0.2} \geq 690$ MPa, and tensile strength range R_m = 770–940 MPa, given in EN 10025-6 standard. It is indicative that measured strength values show certain deviations across the tested material volume, which are generally due to BM material through-thickness inhomogeneity (Figure 11). In AW condition, the yield strength range is $R_{p0.2}$ = 683.4 to 811.2 MPa (15.7% change), while the tensile strength range R_m = 774.7 to 862.2 MPa (10.2% change), with similar trends also visible in other PWHT conditions. These results should be taken into account when comparing the influence of PWHT, since, through considering the small statistical test sample (3 specimens) alone, it can be wrongly concluded that there are no temperature changes.

Table 5. Tensile testing properties of S690QL1 steel (BM), L—longitudinal direction.

Specimen Designation	Location	PWHT Cycle	$R_{p0.2}$ [MPa]	R_m [MPa]	E [GPa]	A_5 [%]
TT-BM 1E1	BM	E (AW)	683.4	774.7	162.9	18.44
TT-BM 1E2	BM	E (AW)	715.2	793.9	196.6	17.71
TT-BM 1E3	BM	E (AW)	811.2	862.2	182.5	15.99
TT-BM 1A1	BM	A (max. 400 °C)	753.9	810.6	272.2	16.34
TT-BM 1A2	BM	A (max. 400 °C)	725.6	802.1	225.7	16.56
TT-BM 1A3	BM	A (max. 400 °C)	792.5	851.5	228.9	18.03
TT-BM 1B1	BM	B (max. 530 °C)	763.9	822.6	295.6	19.50
TT-BM 1B2	BM	B (max. 530 °C)	750.3	826.3	205.0	14.92
TT-BM 1B3	BM	B (max. 530 °C)	806.3	866.3	369.5	18.54
TT-BM 1C1	BM	C (max. 550 °C)	722.2	810.0	236.9	15.37
TT-BM 1C2	BM	C (max. 550 °C)	700.9	780.5	224.8	17.32
TT-BM 1C3	BM	C (max. 550 °C)	801.3	863.6	195.6	16.77
TT-BM 1D1	BM	D (max. 600 °C)	787.1	862.9	230.7	18.36
TT-BM 1D2	BM	D (max. 600 °C)	798.0	861.1	243.0	17.64
TT-BM 1D3	BM	D (max. 600 °C)	765.1	831.1	171.6	19.04

ASTM E8 specimen D = 4 mm, M8 threaded ends (specimen group 1).

Table 6. Tensile testing properties of S690QL1 steel (BM), T—transverse direction.

Specimen Designation	Location	PWHT Cycle	$R_{p0.2}$ [MPa]	R_m [MPa]	E [GPa]	A_5 [%]
TT-BM 4E1	BM	E (AW)	796.0	856.8	221.9	16.49
TT-BM 4E2	BM	E (AW)	714.0	795.3	336.6	19.50
TT-BM 4E3	BM	E (AW)	805.2	859.9	210.3	17.73
TT-BM 4A1	BM	A (max. 400 °C)	802.6	861.3	212.8	18.13
TT-BM 4A2	BM	A (max. 400 °C)	798.0	848.6	246.0	18.00
TT-BM 4A3	BM	A (max. 400 °C)	690.6	766.8	212.3	15.73
TT-BM 4B1	BM	B (max. 530 °C)	801.0	860.9	260.0	16.58
TT-BM 4B2	BM	B (max. 530 °C)	732.5	815.2	290.9	16.18
TT-BM 4B3	BM	B (max. 530 °C)	793.9	854.8	432.0	15.98
TT-BM 4C1	BM	C (max. 550 °C)	795.0	856.9	256.2	19.29
TT-BM 4C2	BM	C (max. 550 °C)	694.9	768.3	234.8	18.98
TT-BM 4C3	BM	C (max. 550 °C)	789.9	850.9	205.6	18.25
TT-BM 4D1	BM	D (max. 600 °C)	806.8	868.1	264.3	18.49
TT-BM 4D2	BM	D (max. 600 °C)	807.5	865.2	278.8	17.97
TT-BM 4D3	BM	D (max. 600 °C)	772.6	833.3	172.8	18.51

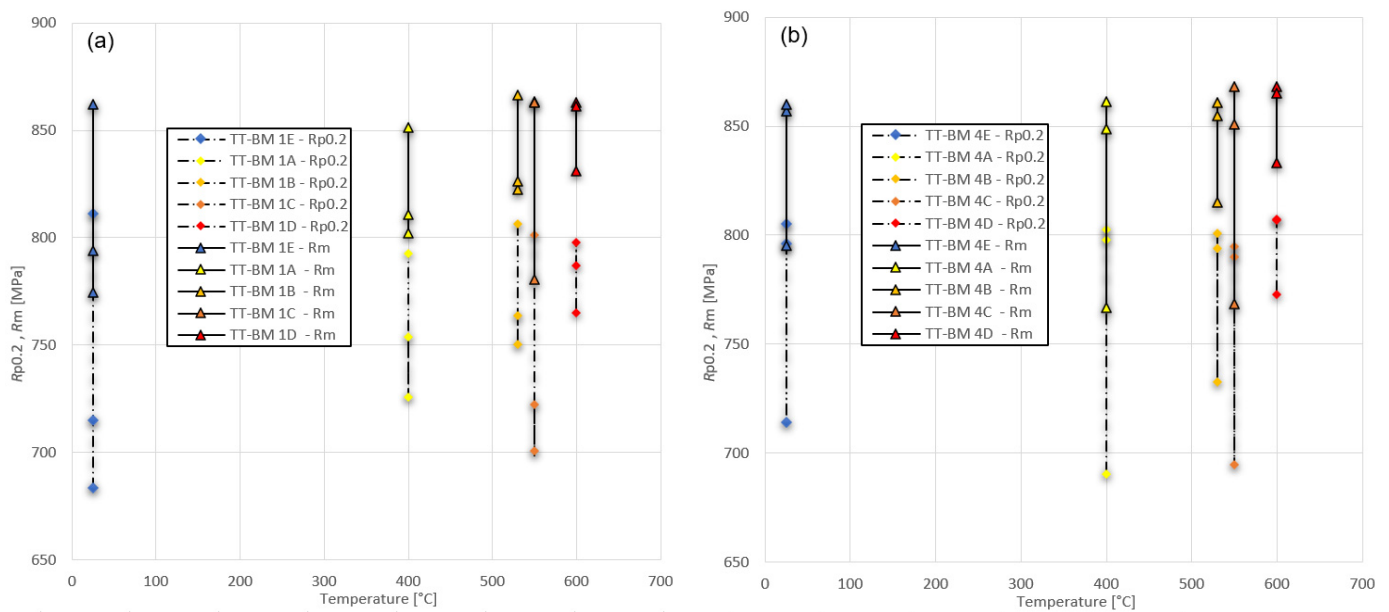ASTM E8 specimen D = 4 mm, M8 threaded ends (specimen group 4).

Figure 11. Tensile properties $R_{\text{p0.2}}$ and R_{m}. Deviation of samples from BM zone: (**a**) L—longitudinal direction; (**b**) T—transverse direction.

Several representative stress–strain diagrams of S690QL1 steel BM are used to describe the relationship between tensile properties and PWHT cycles (Figure 12), with trends of $R_{\text{p0.2}}$ and R_{m} to temperature dependence (Figure 13). Observing the temperature dependence, the change in tensile properties from AW condition to Cycle D is as follows (Figure 13). In L direction, the range of the decrease in values is $R_{\text{p0.2}}$ = 811.2 to 765.1 MPa (5.7% decrease) and R_{m} = 862.2 to 831.1 MPa (3.6% decrease). In T direction, the range of the decrease in values is $R_{\text{p0.2}}$ = 805.2 to 772.6 MPa (4.0% decrease) and R_{m} = 859.9 to 833.3 MPa (3.1% decrease). Looking at the stress–strain curves, it can be observed that elongation generally increases, making the material more ductile. It can be generally concluded that stress–strain properties of BM were not = significantly compromised via exposure to PWHT thermal cycles at temperatures below 600 °C.
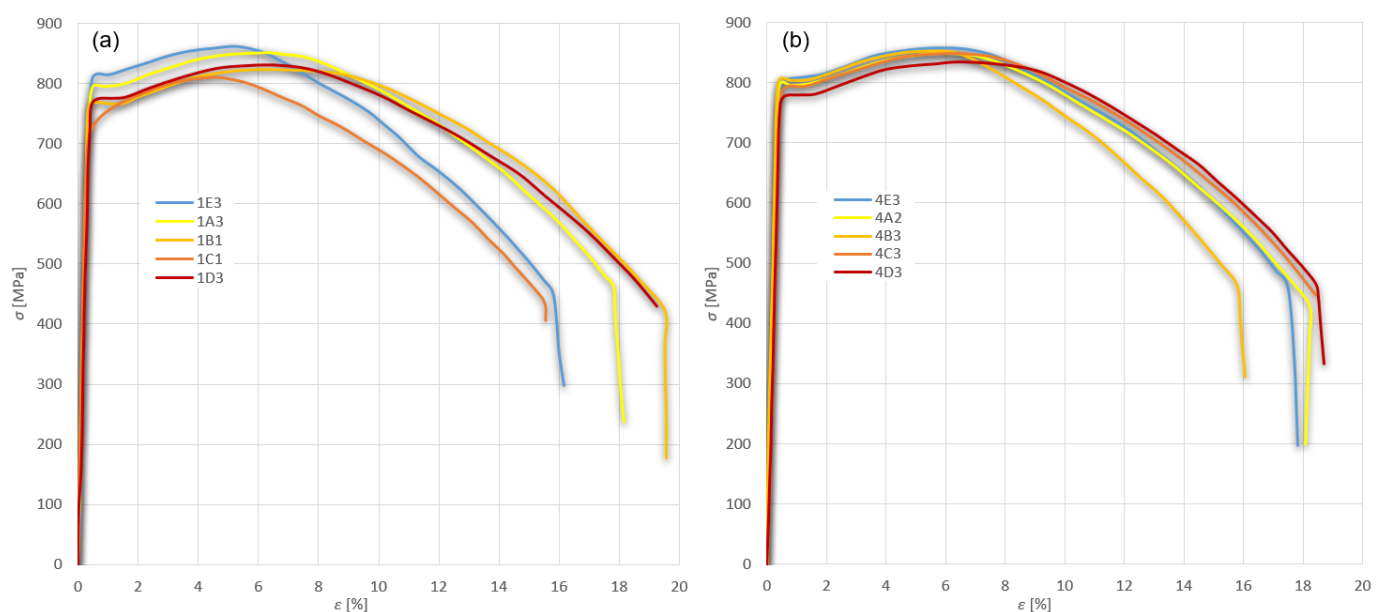

Figure 12. Stress–strain diagrams of S690QL1 steel (BM): (**a**) L—longitudinal direction; (**b**) T—transverse direction.
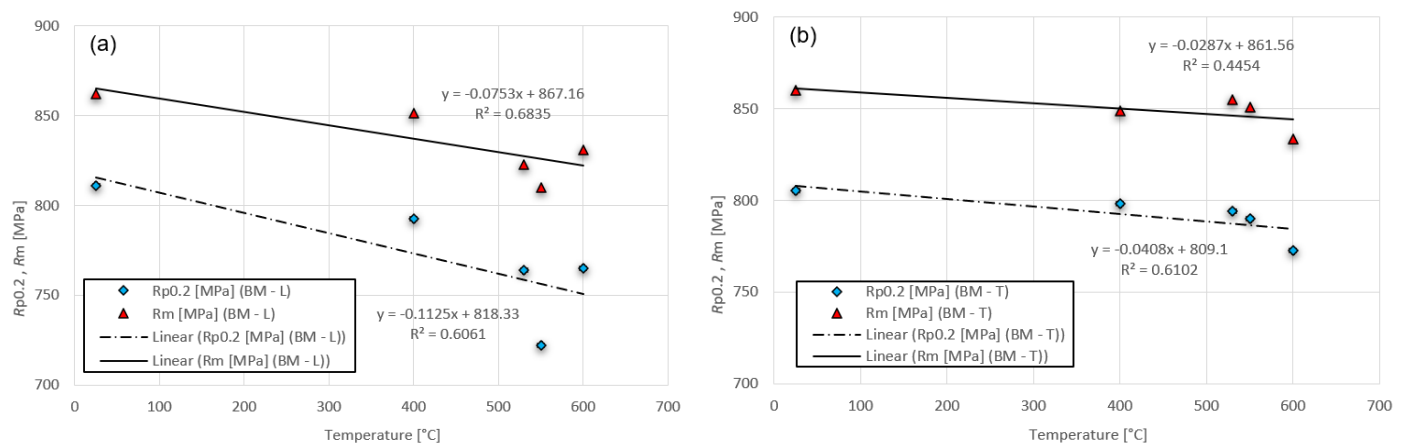
Figure 13. Tensile properties $R_{p0.2}$ and R_m obtained from BM stress–strain curves shown in Figure 12. Trends of temperature dependence: (**a**) L—longitudinal direction; (**b**) T—transverse direction.

Strength testing of WM and HAZ (S690QL1+ Mn3Ni1CrMo welded joint) is performed in L direction only; the results are given in Table 7. In condition after welding (AW), for WM, the yield strength range is $R_{p0.2}$ = 714.5 to 821.9 MPa (13.9% change), and the tensile strength range is R_m = 877.9 to 928.3 MPa (5.5% change). For HAZ, the yield strength range is $R_{p0.2}$ = 736.1 to 990.4 MPa (29.4% change), and the tensile strength range is R_m = 855.1 to 1019.0 MPa (17.5% change). Due to the tensile specimens' size, experimental investigation is limited to generalized HAZ volume, which is not able to address the following individual HAZ segments: coarse-grained zone (CGHAZ), fine-grained zone (FGHAZ), etc. Consequently, a significant deviation of measured $R_{p0.2}$ and R_m values is present inside the HAZ region. Multi-pass welding with generated interpass temperatures acting on all weld passes, except the final ones (Figure 1: 19 and 22), further contributes to the deviation in the results (Figure 14).
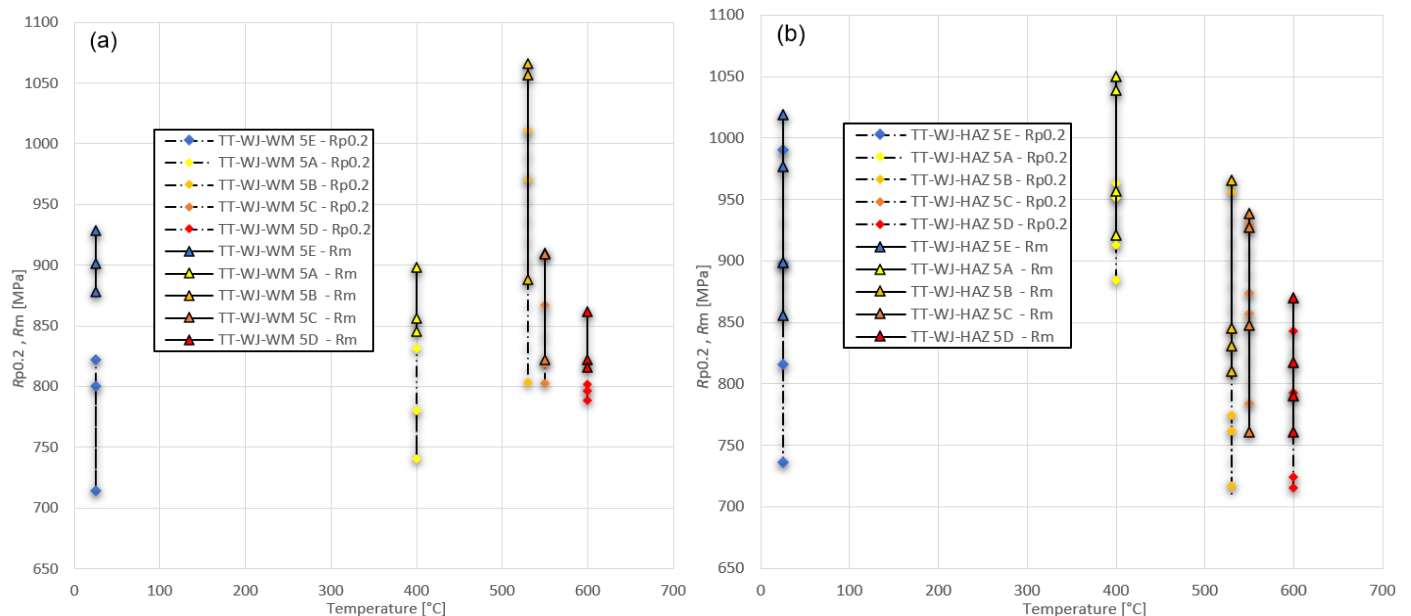

Figure 14. Tensile properties $R_{p0.2}$ and R_m. Deviation of samples from welded joint zone: (**a**) WM in L direction; (**b**) HAZ in L direction.

Table 7. Tensile testing properties of S690QL1+ Mn3Ni1CrMo welded joint (WM, HAZ), L— longitudinal direction.

Specimen Designation	Location	PWHT Cycle	$R_{p0.2}$	R_m	E	A_5
			[MPa]	[MPa]	[GPa]	[%]
TT-WJ 5E1	HAZ	E (AW)	990.4	1019.0	257.5	12.58
TT-WJ 5E2	WM	E (AW)	800.7	901.1	272.1	18.14
TT-WJ 5E3	WM	E (AW)	714.5	877.9	237.7	14.42
TT- WJ 5E4	HAZ	E (AW)	736.1	899.0	215.7	16.33
TT-WJ 5E5	HAZ	E (AW)	897.7	977.0	371.0	14.33
TT-WJ 5E6	WM	E (AW)	821.9	928.3	222.7	13.00
TT-WJ 5E7	HAZ	E (AW)	815.5	855.4	227.7	15.25
TT-WJ 5A1	HAZ	A (max. 400 °C)	884.5	921.3	223.5	11.67
TT-WJ 5A2	WM	A (max. 400 °C)	780.4	845.7	204.9	16.33
TT-WJ 5A3	WM	A (max. 400 °C)	740.2	856.5	184.9	14.65
TT-WJ 5A4	HAZ	A (max. 400 °C)	963.4	1050.0	201.6	12.92
TT-WJ 5A5	HAZ	A (max. 400 °C)	951.7	1039.0	196.0	14.11
TT-WJ 5A6	WM	A (max. 400 °C)	831.1	898.0	201.7	15.25
TT-WJ 5A7	HAZ	A (max. 400 °C)	913.2	957.0	206.7	16.92
TT-WJ 5B1	HAZ	B (max. 530 °C)	955.8	965.7	155.6	16.83
TT-WJ 5B2	WM	B (max. 530 °C)	1011.0	1066.0	216.7	16.17
TT-WJ 5B3	WM	B (max. 530 °C)	970.7	1057.0	201.4	16.67
TT-WJ 5B4	HAZ	B (max. 530 °C)	716.6	810.5	213.6	19.68
TT-WJ 5B5	HAZ	B (max. 530 °C)	774.6	845.1	375.9	18.50
TT-WJ 5B6	WM	B (max. 530 °C)	803.5	888.0	219.3	16.03
TT-WJ 5B7	HAZ	B (max. 530 °C)	761.5	831.1	251.9	21.75
TT-WJ 5C1	HAZ	C (max. 550 °C)	929.5	987.5	208.9	20.00
TT-WJ 5C2	WM	C (max. 550 °C)	802.5	860.0	176.7	13.00
TT-WJ 5C3	WM	C (max. 550 °C)	818.9	909.5	212.7	17.42
TT-WJ 5C4	HAZ	C (max. 550 °C)	873.7	927.7	295.9	18.67
TT-WJ 5C5	HAZ	C (max. 550 °C)	783.8	847.4	336.8	16.00
TT-WJ 5C6	WM	C (max. 550 °C)	867.3	908.9	200.7	17.33
TT-WJ 5C7	HAZ	C (max. 550 °C)	856.9	938.3	341.6	20.92
TT-WJ 5D1	HAZ	D (max. 600 °C)	715.4	761.2	301.2	13.00
TT-WJ 5D2	WM	D (max. 600 °C)	796.4	822.3	194.5	16.21
TT-WJ 5D3	WM	D (max. 600 °C)	788.7	815.8	232.6	14.57
TT-WJ 5D4	HAZ	D (max. 600 °C)	723.9	790.2	334.1	18.00
TT-WJ 5D5	HAZ	D (max. 600 °C)	792.4	817.4	328.8	15.42
TT-WJ 5D6	WM	D (max. 600 °C)	801.7	861.8	256.3	15.17
TT-WJ 5D7	HAZ	D (max. 600 °C)	842.7	870.2	270.5	13.67

ASTM E8 specimen D = 2.5 mm, M4 threaded ends (specimen group 5).

Several representative stress–strain diagrams of the S690QL1+ Mn3Ni1CrMo welded joint (WM, HAZ) are used to describe the relationship between tensile properties and PWHT cycles (Figure 15), with trends of $R_{p0.2}$ and R_m used to temperature dependence (Figure 16). Similarly to the previous case that investigated the influence of PWHT cycle holding temperature increases on BM strength properties, WM and HAZ strength values also show a decreasing trend, while elongation increases. Observing the temperature dependence, the change in tensile properties from AW condition to Cycle D is as follows (Figure 16). For WM, the range of the decrease in values is $R_{p0.2}$ = 821.9 to 788.7 MPa (4.0% decrease) and R_m = 928.3 to 815.8 MPa (12.1% decrease). For HAZ, the range of the decrease in values is $R_{p0.2}$ = 990.4 to 792.4 MPa (20.0% decrease) and R_m = 1019.0 to 817.4 MPa (19.8% decrease). After exposure to PWHT thermal cycles at temperatures below 600 °C, stress–strain properties of WM and HAZ exhibit substantial degradation, and the possibility of welded joints being exploited in the scope of welded structures should be given special consideration.
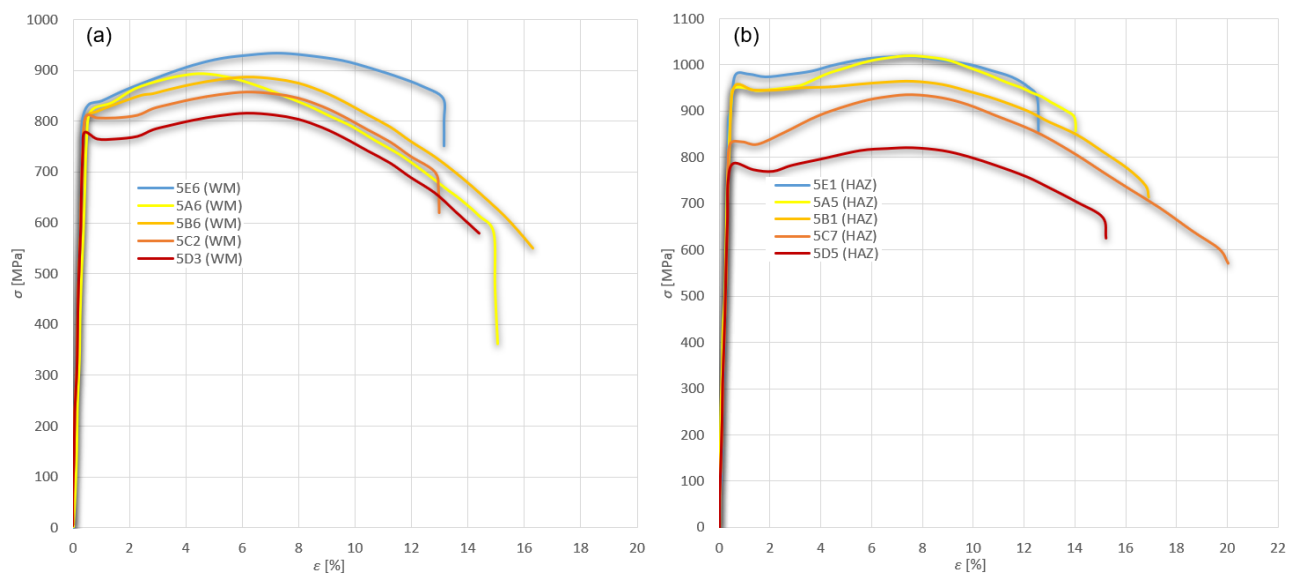
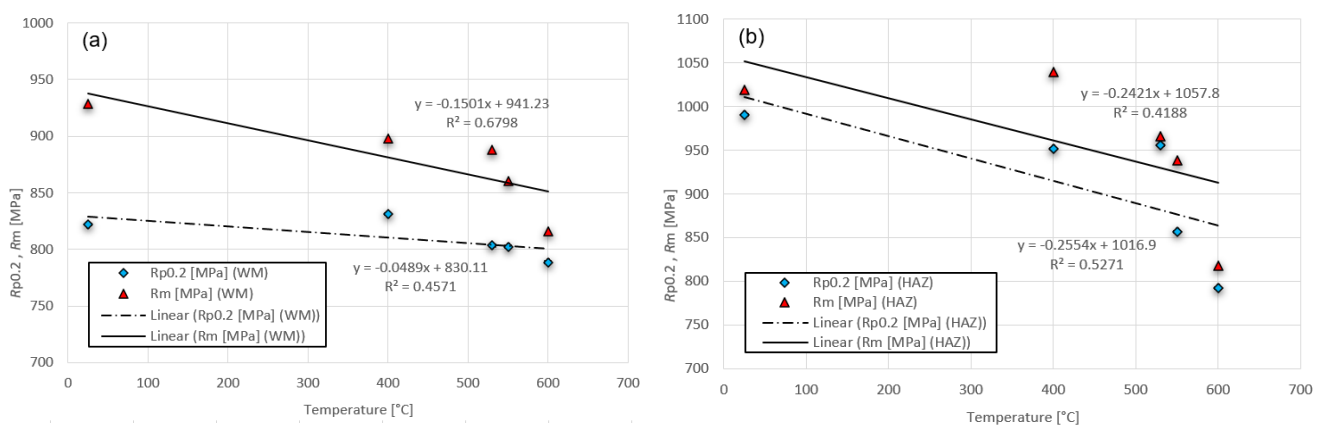**Figure 15.** Stress–strain diagrams of S690QL1 steel: (**a**) WM in L direction; (**b**) HAZ in L direction.

Figure 16. Tensile properties $R_{p0.2}$ and R_m obtained from stress–strain curves shown in Figure 15. Trends of temperature dependence: (**a**) WM in L direction; (**b**) HAZ in L direction.

It is important to note that the results of tensile testing show a minor or major degree of scatter, with the exact results varying depending on the tested volume of the welded joint and the dimensions of tensile specimen used. Using the ASTM E8 specimen $D = 4$ mm with M8 threaded ends in BM material volume shows the highest degree of confidence and repeatability. Using the ASTM E8 specimen $D = 2.5$ mm with M4 threaded ends in WM and HAZ entails certain problems. Due to the small specimen size, manufacturing problems and imperfections are present during machining, which leads to measurement deviations. In addition to this issue, the previously mentioned deviations in mechanical properties within the material itself, and its inability to capture the HAZ segments properties individually, instead doing so on a general level, lead to further measurement unreliability.

In the author's opinion, the measured tensile test results show sufficiently good material behavior under the PWHT thermal cycles exposure that we can make final conclusions about the applicability of such welded joints in creating real engineering structures. As previously mentioned, S690QL1 HSS BM retained its stress–strain properties under exposure to temperatures below 600 °C, while welded joint (WM and HAZ), using the Mn3Ni1CrMo filler material, exhibited substantial degradation in such properties. For a more detailed analysis of the HAZ region, which is beyond the scope of this paper, it is recommended to use alternative experimental methods (e.g., Mini Tensile Specimens (MTS) [32,33] or the Profilometry-based Indentation Plastometry (PIP) method [34,35]).

3.1.2. Impact Testing

Impact Charpy V-notch testing is used to determine the absorbed energy (KV_2) at a temperature of +22 °C. The fracture surface of Charpy test pieces is examined to determine the percentage of shear fracture (*FA*) in contrast to cleavage (brittle) fracture. In general, the increase in shear fracture percentage also indicates the increase in notch toughness of the material. Since *FA* has a very subjective rating, it is used for general review purposes only. As with the previous tensile test, AW and four different PWHT material conditions are tested. For each material condition, three impact specimens are tested in order to gain additional levels of confidence. The BM HSS steel S690QL1 is tested in transverse-longitudinal (T-L) direction, meaning the specimen is positioned transversely to the welded joint, while the notch itself is oriented in longitudinal direction. The test results are given in Table 8. Impact testing of BM in condition After Welding (AW) determined that the average absorbed energy is KV_2 = 191.30 J. With regard to through-thickness material behavior in BM, in condition After Welding (AW), the absorbed energy range is KV_2 = 175.2 to 203.4 J (16.1% change). To determine the relationship between individual PWHT cycles and absorbed energy, representative KV_2 values are chosen. They correspond to the values obtained via impact testing (Table 8) samples located in the middle of the BM cross-section. Observing the temperature dependence, the change in absorbed energy from AW condition to Cycle D is as follows (Figure 17). For BM T-L testing, the decrease in values is KV_2 = 175.2 to 145.2 J (17.1% decrease). The percentage of all specimens' shear fracture is not significantly affected by thermal cycles and retains an average value of 47.93%. In general, it can be concluded that impact properties of BM exhibit a decreasing trend, but are not significantly compromised via exposure to PWHT thermal cycles at temperatures below 600 °C.

Impact testing of WM, FL, and HAZ (S690QL1+ Mn3Ni1CrMo welded joint) is also performed in T-L direction, with results for WM given in Table 9, for FL in Table 10, and for HAZ in Table 11.

Table 8. Impact testing properties of S690QL1 steel (BM), T-L—transverse-longitudinal direction.

Specimen Designation	Location	PWHT Cycle	KV_2	FA
			[J]	[%]
IT-BM 2E1	BM	E (AW)	203.40	51
IT-BM 2E2	BM	E (AW)	175.20	55
IT-BM 2E3	BM	E (AW)	195.40	39
IT-BM 2A1	BM	A (max. 400 °C)	196.00	47
IT-BM 2A2	BM	A (max. 400 °C)	207.15	51
IT-BM 2A3	BM	A (max. 400 °C)	183.90	51
IT-BM 2B1	BM	B (max. 530 °C)	183.90	47
IT-BM 2B2	BM	B (max. 530 °C)	177.40	51
IT-BM 2B3	BM	B (max. 530 °C)	181.45	47
IT-BM 2C1	BM	C (max. 550 °C)	182.40	47
IT-BM 2C2	BM	C (max. 550 °C)	189.35	47
IT-BM 2C3	BM	C (max. 550 °C)	175.30	45
IT-BM 2D1	BM	D (max. 600 °C)	193.55	47
IT-BM 2D2	BM	D (max. 600 °C)	145.20	47
IT-BM 2D3	BM	D (max. 600 °C)	190.90	47

Charpy V-notch specimen (specimen group 2); KV_2: absorbed energy for a V-notch test piece using a 2 mm striker; *FA*: shear-fracture appearance.

Impact testing in the condition after welding (AW) determined the average absorbed energy of WM to be KV_2 = 127.70 J, of FL to be KV_2 = 129.20 J, and of HAZ to be KV_2 = 124.90 J. With regard to through-thickness material behavior in WM, FL, and HAZ, in condition after welding (AW), the absorbed energy range for WM is KV_2 = 107.05 to 160.20 J (49.6% change), for FL is KV_2 = 113.85 to 141.35 J (24.2% change), and for HAZ is KV_2 = 94.85 to 172.30 J (81.7% change). The most noticeable change is the significant drop in absorbed energy values in the top and bottom parts of welded joint cross section, which corresponds to fill

and cover passes. In all welded joint regions, and for all PWHT cycles exposure, the highest absorbed energy values are determined in the middle of the welded joint cross-section, which corresponds to root passes. Such behavior is present in multi-pass welding, where the interpass heat input reheats the previously welded passes. This outcome is in contrast to the behavior of BM, which has mostly uniform through-thickness properties. To determine the relationship between individual PWHT cycles and absorbed energy, as in case of BM, representative KV_2 values are also chosen for WM, FL, and HAZ. They correspond to the values obtained using impact testing (Tables 9–11) samples located in the middle of the BM cross-section. Observing the temperature dependence, the change in absorbed energy from AW condition to Cycle D is as follows (Figure 17). For WM T-L testing, the decrease in values is KV_2 = 160.2 to 118.8 J (25.8% decrease); for FL T-L testing, the decrease in values is KV_2 = 132.4 to 115.8 J (12.5% decrease); and for HAZ T-L testing, the decrease in values is KV_2 = 172.3 to 171.2 J (0.6% decrease) Shear fracture has an average value in WM of 44%, in FL of 47.67%, and in HAZ of 43%. It can be concluded that BM and welded joints (WM, FL and HAZ) retain sufficiently good impact properties under exposure to temperatures below 600 °C, which are present during the PWHT thermal cycles.

3.1.3. Hardness Measurements

Hardness measurements are performed to determine HV values in the welded joint's cross-sectional area. The results of hardness distribution along the top (1–2mm from top surface), center (2–20 mm centerline), and bottom (3–2mm from bottom surface) measurement lines (Figure 9), in relation to the PWHT thermal cycles influence, are given (Figure 18). In order to investigate the hardness variations throughout the complete welded joint, measurements are taken in BM, HAZ, and WM regions. Diagrams show hardness HV values in relation to left- and right-side distance from the weld's vertical centerline.
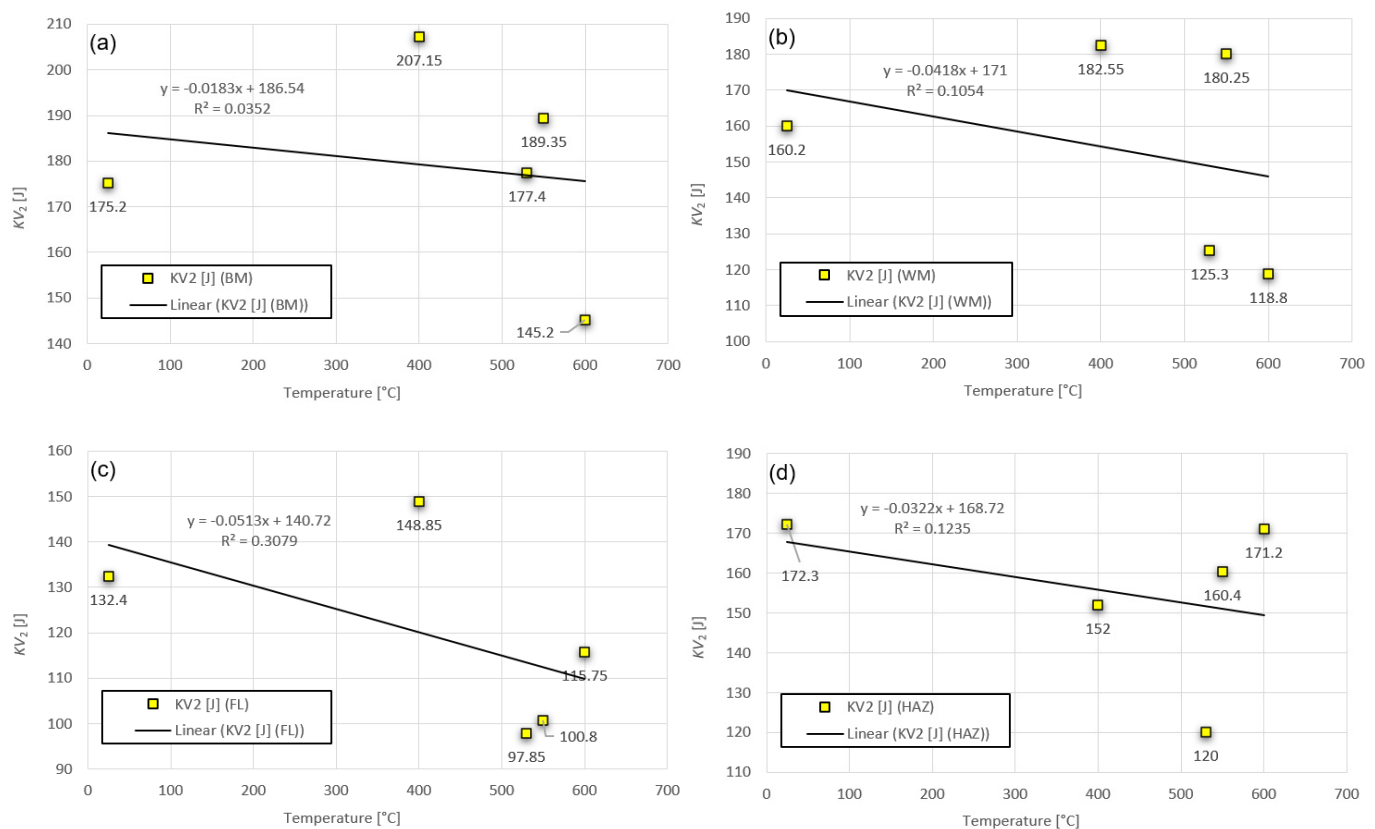

Figure 17. Impact testing properties KV2 of S690QL1+ Mn3Ni1CrMo-welded joint from samples located in middle of cross-section. Trends of temperature dependence: (**a**) BM in T-L direction; (**b**) WM in T-L direction; (**c**) FL in T-L direction; (**d**) HAZ in T-L direction.

Table 9. Impact testing properties of S690QL1+ Mn3Ni1CrMo-welded joint (WM), T-L—transverse-longitudinal direction.

Specimen Designation	Location	PWHT Cycle	KV_2 [J]	FA [%]
IT-WJ 7E1	WM	E (AW)	107.05	30
IT-WJ 7E2	WM	E (AW)	160.20	36
IT-WJ 7E3	WM	E (AW)	115.90	35
IT-WJ 7A1	WM	A (max. 400 °C)	105.50	55
IT-WJ 7A2	WM	A (max. 400 °C)	182.55	51
IT-WJ 7A3	WM	A (max. 400 °C)	112.95	44
IT-WJ 7B1	WM	B (max. 530 °C)	88.40	56
IT-WJ 7B2	WM	B (max. 530 °C)	125.30	39
IT-WJ 7B3	WM	B (max. 530 °C)	74.40	56
IT-WJ 7C1	WM	C (max. 550 °C)	79,00	52
IT-WJ 7C2	WM	C (max. 550 °C)	180,25	31
IT-WJ 7C3	WM	C (max. 550 °C)	68.00	39
IT-WJ 7D1	WM	D (max. 600 °C)	89.25	48
IT-WJ 7D2	WM	D (max. 600 °C)	118.80	44
IT-WJ 7D3	WM	D (max. 600 °C)	64.60	44

Charpy V-notch specimen (specimen group 7).

Table 10. Impact testing properties of S690QL1+ Mn3Ni1CrMo-welded joint (FL), T-L—transverse-longitudinal direction.

Specimen Designation	Location	PWHT Cycle	KV_2 [J]	FA [%]
IT-WJ 8E1	FL	E (AW)	113.85	39
IT-WJ 8E2	FL	E (AW)	132.40	47
IT-WJ 8E3	FL	E (AW)	141.35	47
IT-WJ 8A1	FL	A (max. 400 °C)	94.45	59
IT-WJ 8A2	FL	A (max. 400 °C)	148.85	47
IT-WJ 8A3	FL	A (max. 400 °C)	114.85	47
IT-WJ 8B1	FL	B (max. 530 °C)	93.70	52
IT-WJ 8B2	FL	B (max. 530 °C)	97.85	55
IT-WJ 8B3	FL	B (max. 530 °C)	91.10	55
IT-WJ 8C1	FL	C (max. 550 °C)	84.15	51
IT-WJ 8C2	FL	C (max. 550 °C)	100.80	55
IT-WJ 8C3	FL	C (max. 550 °C)	75.40	43
IT-WJ 8D1	FL	D (max. 600 °C)	76.60	51
IT-WJ 8D2	FL	D (max. 600 °C)	115.75	20
IT-WJ 8D3	FL	D (max. 600 °C)	101.45	47

Charpy V-notch specimen (specimen group 8).

Table 11. Impact testing properties of S690QL1+ Mn3Ni1CrMo-welded joint (HAZ), T-L— transverse-longitudinal direction.

Specimen Designation	Location	PWHT Cycle	KV_2 [J]	FA [%]
IT-WJ 9E1	HAZ	E (AW)	94.85	48
IT-WJ 9E2	HAZ	E (AW)	172.30	16
IT-WJ 9E3	HAZ	E (AW)	107.60	35
IT-WJ 9A1	HAZ	A (max. 400 °C)	147.05	47
IT-WJ 9A2	HAZ	A (max. 400 °C)	152.00	35
IT-WJ 9A3	HAZ	A (max. 400 °C)	151.50	51
IT-WJ 9B1	HAZ	B (max. 530 °C)	106.85	59
IT-WJ 9B2	HAZ	B (max. 530 °C)	120.00	26
IT-WJ 9B3	HAZ	B (max. 530 °C)	79.65	51

Table 11. *Cont.*

Specimen Designation	Location	PWHT Cycle	KV_2	FA
			[J]	[%]
IT-WJ 9C1	HAZ	C (max. 550 °C)	85.60	55
IT-WJ 9C2	HAZ	C (max. 550 °C)	160.40	27
IT-WJ 9C3	HAZ	C (max. 550 °C)	105.35	39
IT-WJ 9D1	HAZ	D (max. 600 °C)	84.50	62
IT-WJ 9D2	HAZ	D (max. 600 °C)	171.20	35
IT-WJ 9D3	HAZ	D (max. 600 °C)	87.80	59

Charpy V-notch specimen (specimen group 9).
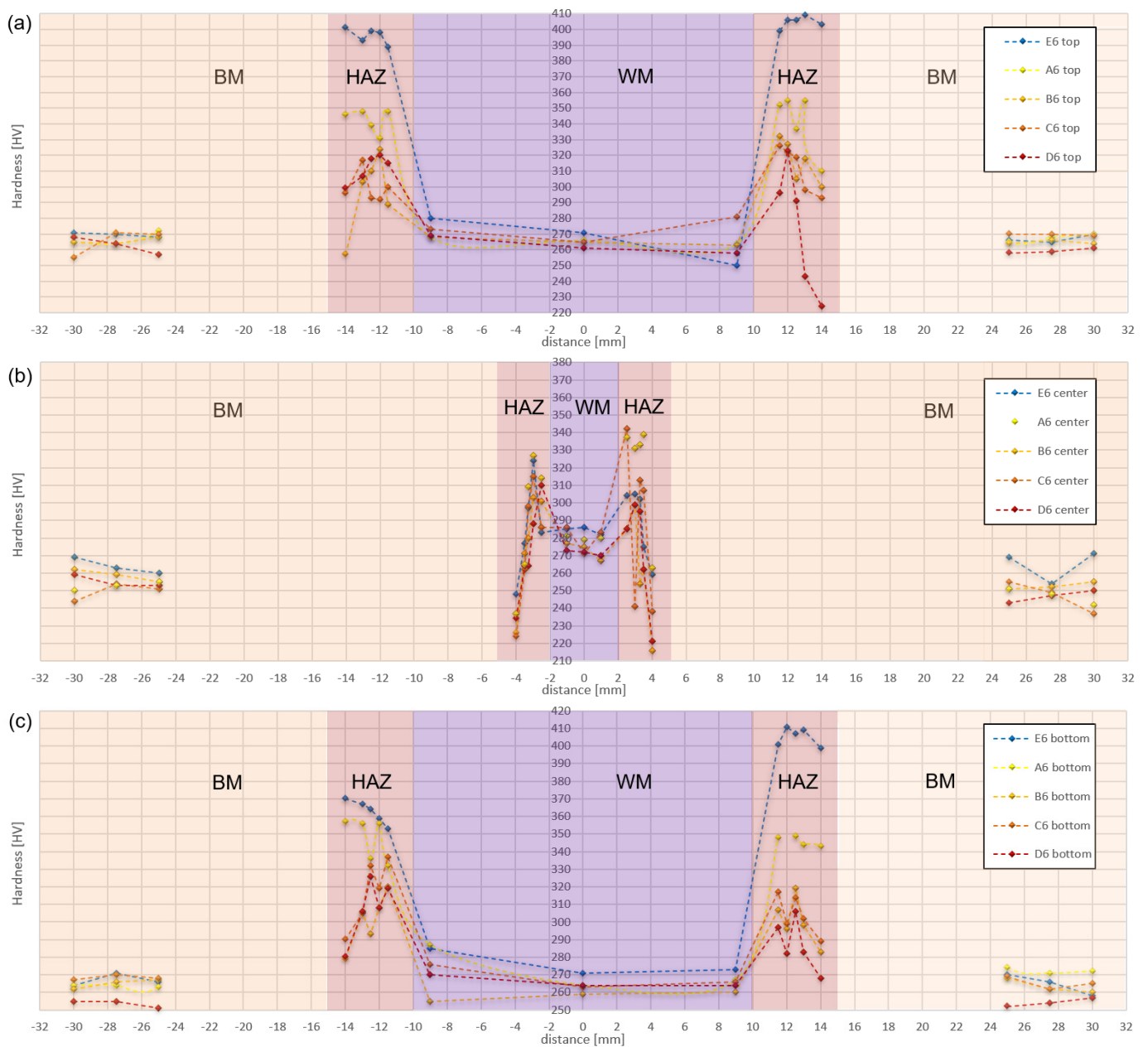
Figure 18. Hardness distribution in welded joint after exposure to PWHT cycles: (**a**) line 1—top; (**b**) line 2—center; (**c**) line 3—bottom.

Hardness testing in condition after welding (AW) determined that the average hardness of BM is 266 HV, of WM is 276 HV, of CGHAZ is 362 HV, and of remaining HAZ

regions is 351 HV. All welded joint regions are susceptible to PWHT thermal cycles exposure, which is reflected in hardness decrease due to temperature increase. This result is indicated in Table 12. Observing the temperature dependence, the changes in hardness from AW condition to Cycle D, according to welded joint regions, are a 4.1% decrease for BM, a 3.2% decrease for WM, a 16.6% decrease for CGHAZ, and a 24.2% decrease for HAZ. These finding correlate well with previously determined stress–strain behavior, where BM retains its properties, while HAZ exhibits substantial degradation in its properties.

Table 12. Hardness properties of welded joint regions in relation to PWHT thermal cycles.

PWHT Cycle	BM	WM	CGHAZ	HAZ
	[HV]	[HV]	[HV]	[HV]
E (AW)	266	276	362	351
A (max. 400 °C)	262	284	338	322
B (max. 530 °C)	262	265	303	277
C (max. 550 °C)	261	274	309	285
D (max. 600 °C)	255	267	302	266

Average hardness properties of each welded joint region are given.

3.2. Metallographic Examination

Metallographic examination is performed to evaluate the macro- and micro-scopic aspects of the X-welded joint. Examinations are performed on joints in AW, as well as four different PWHT cycle conditions, in order to compare and determine possible changes at the material metallographic level.

The X-welded joint is first examined in detail in the As-Welded (AW) condition, using Cycle E to establish the initial material observations. Macroscopic images reveal individual welding passes of multi-pass welding configurations, clearly depicting the boundaries between the primary segments of the welded joint: BM, WM, and HAZ (Figure 19). The fusion line (FL) is also clearly visible, establishing the boundary between WM and HAZ. As can be seen in the macroscopic image, the welded joint is without cracks or any other welding defects. In order to examine the HAZ region in more detail, microstructural examination is performed on a small area marked in the macro picture.
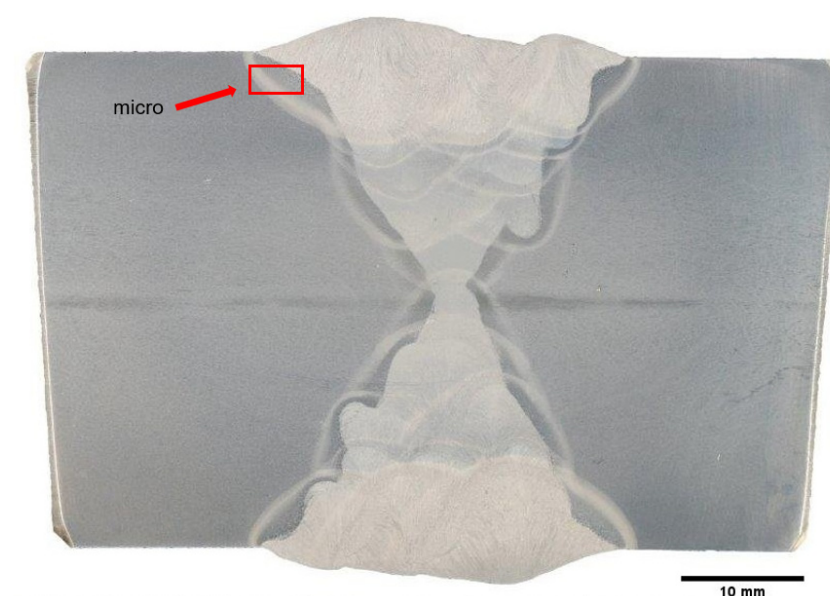

Figure 19. X-welded joint cross-sectional macroscopic image. Cycle E: As-Welded (AW) condition.

HAZ can be generally divided into four individual HAZ segments: the coarse-grained zone (CGHAZ), the fine-grained zone (FGHAZ), the inter-critical zone (ICHAZ), and the

sub-critical zone (SCHAZ), as depicted (Figure 20). In the overheated HAZ area adjacent to WM, significant coarsening of original austenitic grain can be observed. There is a gradual grain refinement towards the BM. The finest polyhedral grain can be found in HAZ with a temperature around A_3, while the zone adjacent to BM has a slightly greater grain size corresponding to HAZ with a temperature between A_1 and A_3. Individual grains can be seen in microstructural color image. The microstructure of S690QL1 BM is fine-grained, composed of martensite (M), and eventually tempered troostite or lower bainite (LB) (Figure 21). However, without electron microscopy, it is not possible to distinguish between the troostite and the lower bainite. The original size of austenitic grain with carbides precipitated along the grain boundaries is visible. The structure of material heated below A_1 is evident in BM. According to ASTM E112, the BM grain size is 11, with a majority of grains being 5–6 μm in diameter. The weld metal WM microstructure matrix is composed of acicular ferrite (AF), with areas resembling upper bainite (UB) morphology (Figure 22).
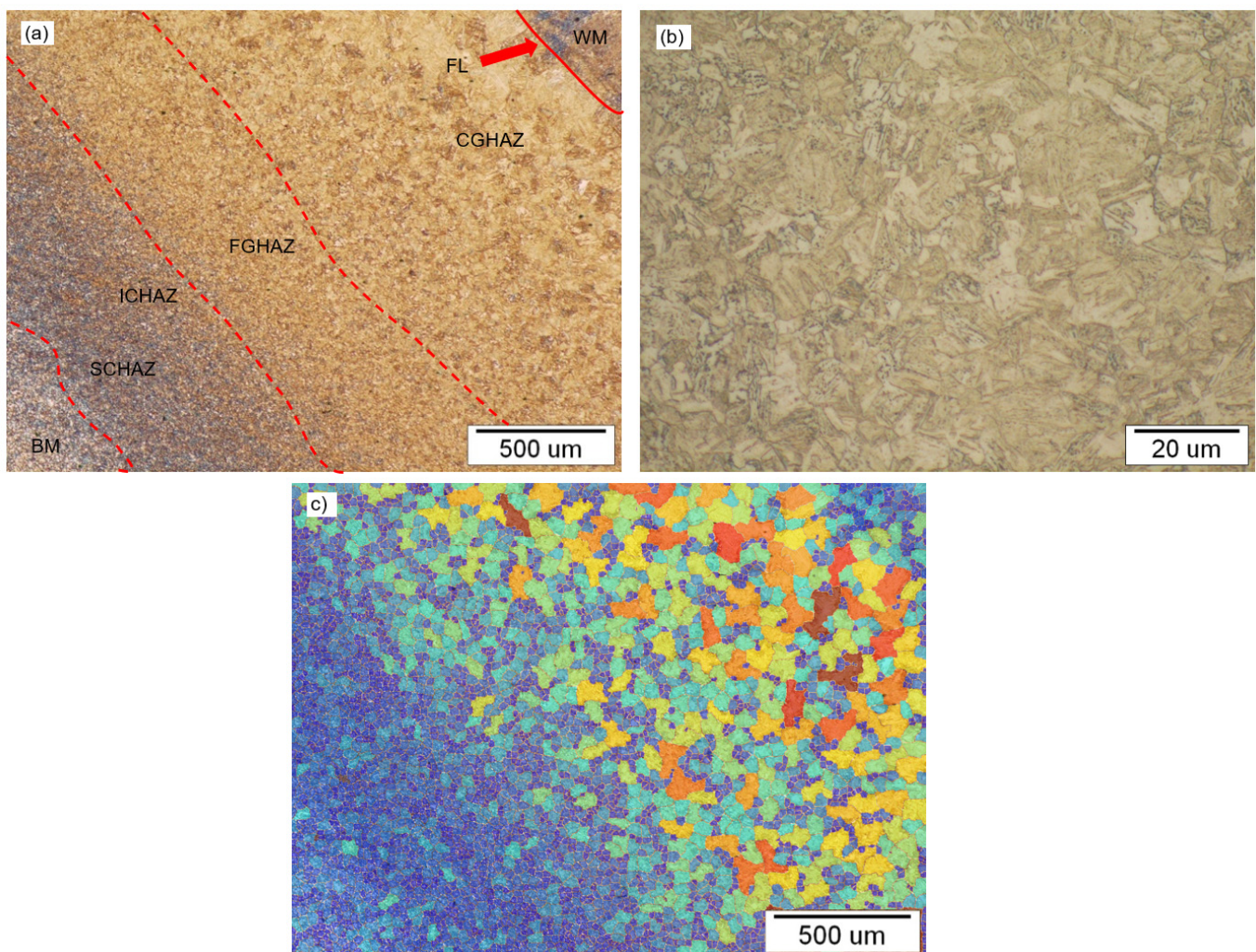
Figure 20. Microstructure of HAZ. Cycle E: As-Welded (AW) condition: (**a**) 500 μm—characteristic HAZ segments; (**b**) 20 μm—grains in CGHAZ; (**c**) 500 μm—grain size color image.

Metallographic examination of X-welded joint material, using the light microscopy, and after the exposure to PWHT thermal cycles, did not reveal significant changes in the material throughout all the specific welded joint segments. Since the BM S690QL1 material is factory-manufactured using the QT process, with rapid water quenching from $\approx 930\ °C$, and subsequent tempering at $\approx 630\ °C$, the exposure to PWHT thermal cycles temperatures below 600 °C had no significant negative impact on the microstructure. In

general, the difference between different PWHT cycles of welded joint is primarily related to dislocation density and precipitation that result in change in mechanical properties. This general behavior of the microstructure is in correlation with the previously conducted mechanical tests of the X-welded joint, indicating that the material retained sufficiently good mechanical properties under the PWHT temperatures below 600 °C. Light microscopy can give an approximate view on the microstructure, which is very similar for AW and all PWHT cycles. For the detailed microstructural analysis, the Transmission Electron Microscopy (TEM) and Scanning Electron Microscopy (SEM) methods should be employed, which is planned in future research on this topic.
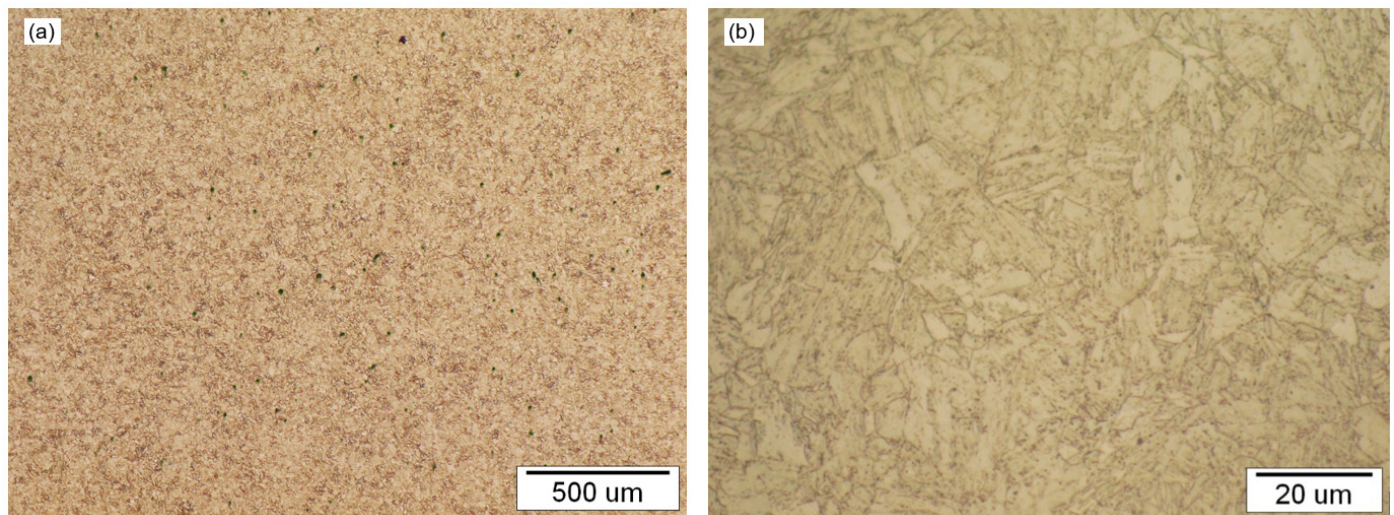
Figure 21. Microstructure of S690QL1 BM. Cycle E: As-Welded (AW) condition: (**a**) 500 μm—general microstructure; (**b**) 20 μm—grains.
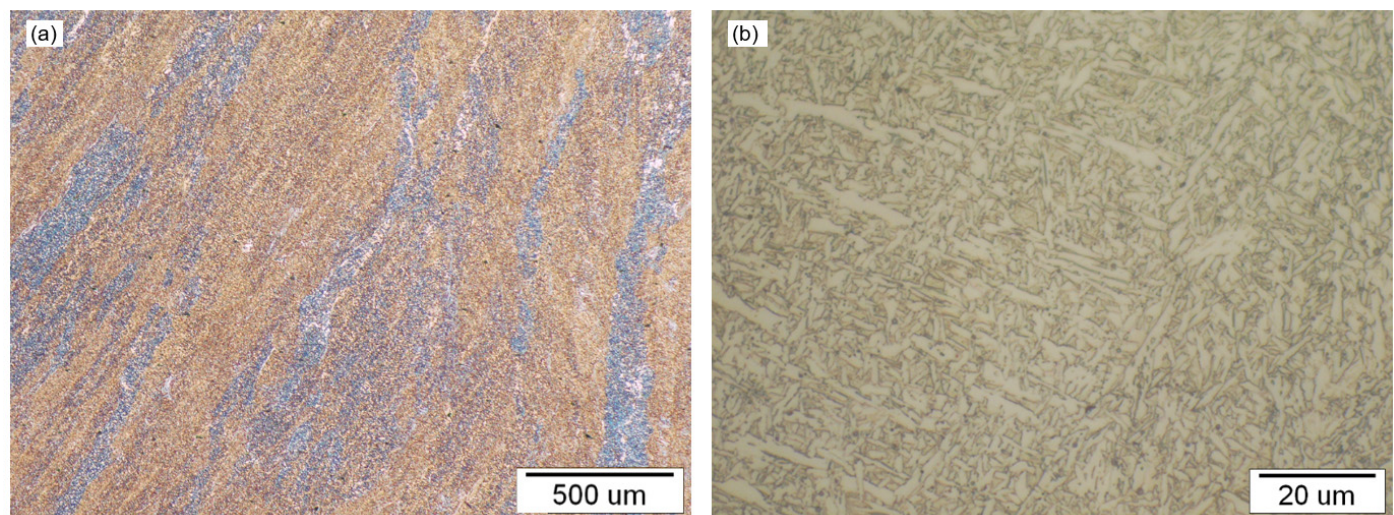
Figure 22. Microstructure of Mn3Ni1CrMo WM. Cycle E: As-Welded (AW) condition: (**a**) 500 μm—general microstructure; (**b**) 20 μm—grains.

3.3. Residual Stress

The influence of PWHT thermal cycles is determined through residual stress quantification. Measurements are performed for AW and four different PWHT cycles, with six points in a linear sequence, located on the top surface of welded specimens. Point 1 is located at the weld centerline, while Point 6 is located 25 mm within the BM (Figure 23).
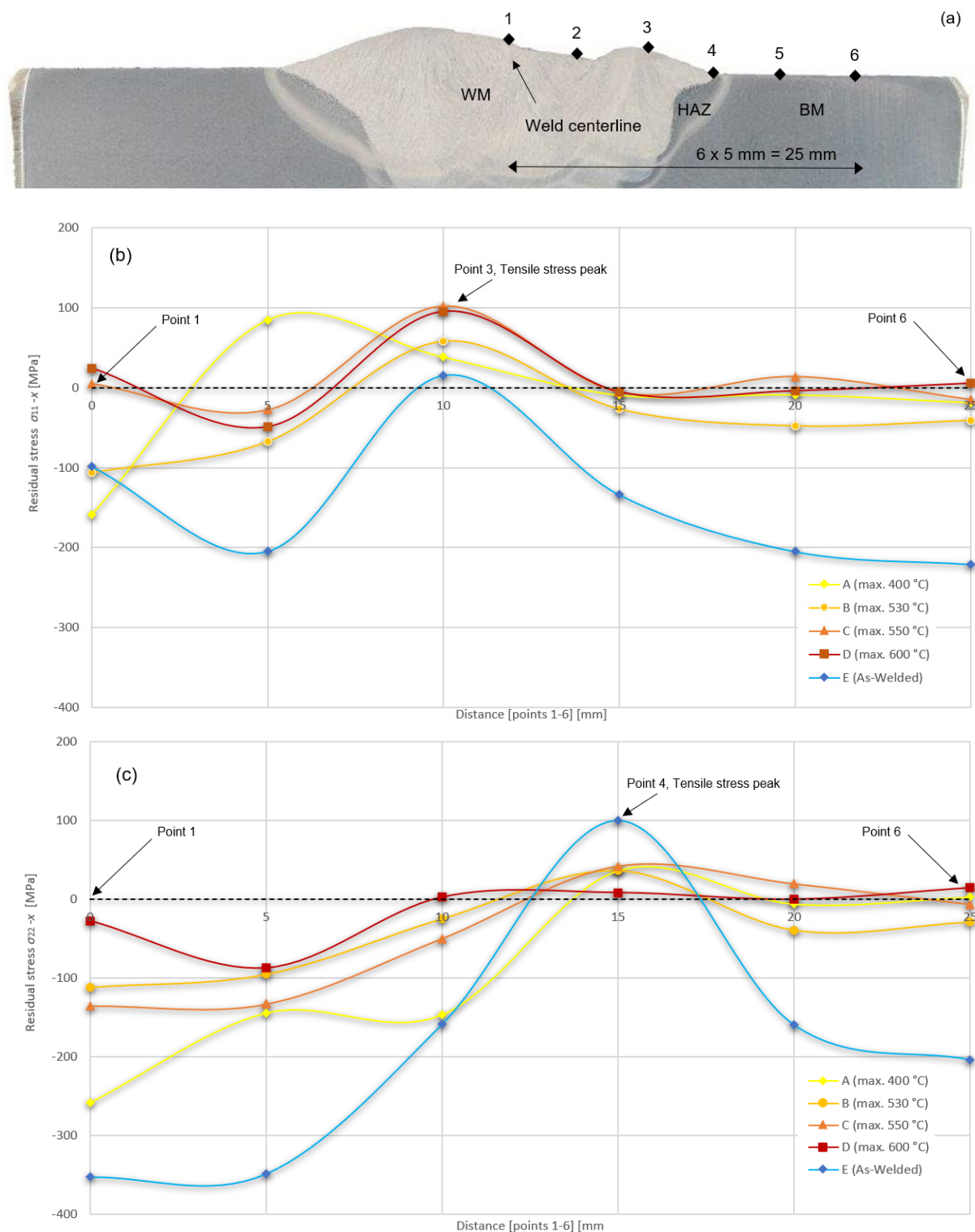
Figure 23. Residual stress measurement: (**a**) X-welded joint cross section with measurement points; (**b**) residual stress components σ_{11} in x direction; (**c**) residual stress components σ_{22} in y direction.

The correlation between residual stress components σ_{11} and σ_{22} and six measurement points is shown in diagram form (Figure 23). For AW condition, stress components σ_{11} in x longitudinal direction exhibit minimum compressive values of -221 MPa, while the maximum tensile stress is 15 MPa. The tensile stress peak is located in Point 3, being 10 mm away from the weld centerline. Stress components σ_{22} in y longitudinal direction exhibit minimum compressive values of -353 MPa, while maximum tensile stress is 99 MPa. The

tensile stress peak is located in Point 4, which is 15 mm from weld centerline. It is evident that significant stress variations are present along the measurement line. With an increase in the temperature of the PWHT cycles, compressive and tensile values approach the zero residual stress line and the peaks flatten out, indicating the correlation between stress relief heat treatment and residual stress reduction. In the author's opinion, for both cases, optimal stress reduction temperature corresponds to PWHT Cycle C (max. 550 °C). For Cycle C, stress components σ_{11} are in a range from -28 to 102 MPa, while stress components σ_{22} are in a range from -136 to 42 MPa. At lower PWHT temperatures, there is an increase in compressive stress values and the formation of peaks. On the other hand, higher PWHT temperatures lead to further stress reduction and stress curve flattening; however, they tend to compromise the mechanical properties of welded joint structure materials, as previously investigated.

The average relative reduction in residual stress in correlation to PWHT temperature is obtained on the basis of values measured at Point 6 for stress components σ_{11} and σ_{22} combined (Figure 24). The relative RS reduction is given in regard to starting Cycle E (AW condition), where the RS reduction is 0%. Relative to Cycle E, the Cycle A (max. 400 °C) achieves 72% RS reduction; Cycle B (max. 530 °C) achieves the 81% RS reduction; Cycle C (max. 550 °C) achieves the 93% RS reduction; and the maximum value is achieved in Cycle D (max. 600 °C), where the RS reduction equals 100%.
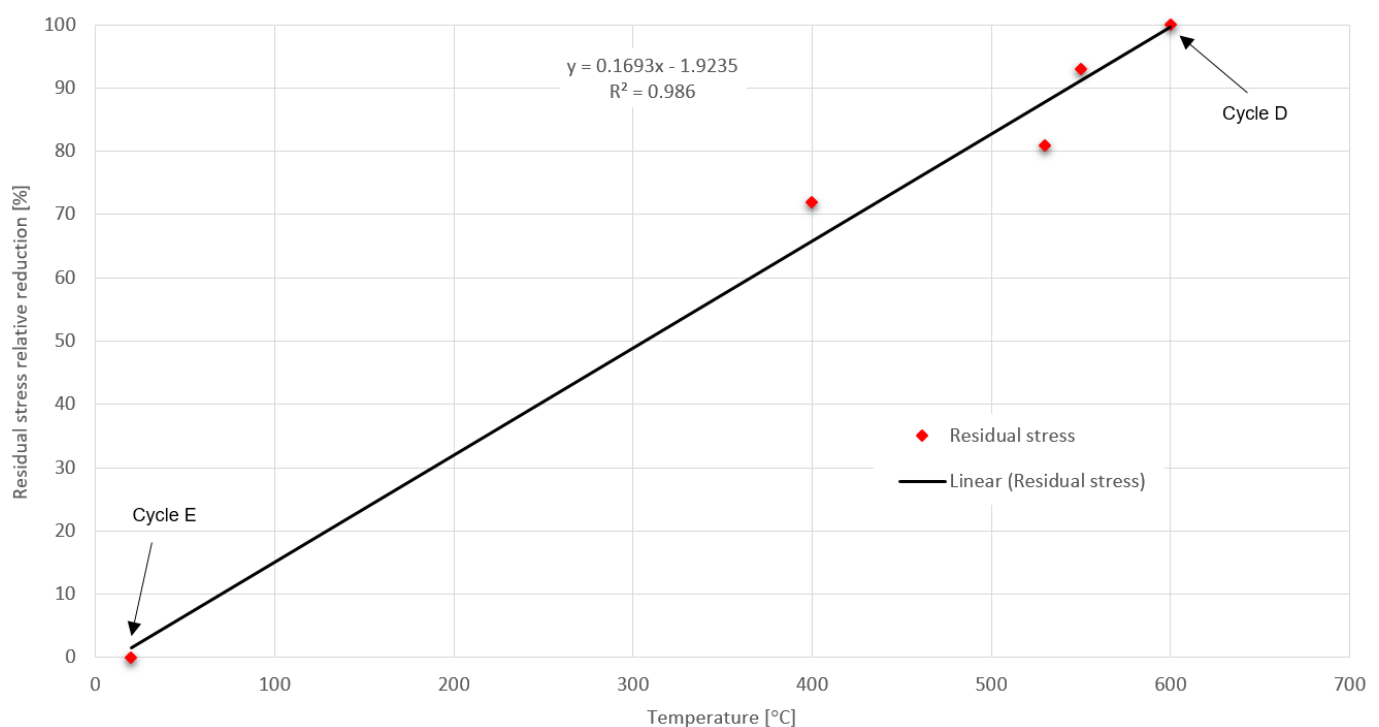

Figure 24. Relative reduction in residual stress in correlation with PWHT temperature.

4. Conclusions

In the scope of this experimental study, the influence of Post-Weld Heat Treatment (PWHT) on multi-pass X-welded joints made from S690QL1 high strength steel is investigated in detail. Welded joints are investigated in either As-Welded (AW) material condition (Cycle E) or after exposure to four different PWHT cycles: Cycle A (max. 400 °C), Cycle B (max. 530 °C), Cycle C (max. 550 °C), and Cycle D (max. 600 °C). Thermal influence on mechanical properties, microstructure, and residual stress are within the expected material grade range. The following conclusions can be drawn:

- S690QL1 steel can generally be subjected to PWHT, while adhering to the limits of the material and process. The highest heat treatment temperatures should be kept

30–40 °C below the steel tempering temperature. The PWHT range, according to manufacturer recommendations, is 530–580 °C.

- Stress–strain properties of BM were not significantly compromised under exposure to temperatures below 600 °C, while the welded joint (WM and HAZ), using the Mn3Ni1CrMo filler material, exhibited substantial degradation of stress–strain properties. The engineering applications of such thermally exposed welded joints should be considered.
- Impact properties of BM and welded joints (WM, FL and HAZ) under exposure to temperatures below 600 °C retained sufficiently good values. Variations in through-thickness properties are evident, especially in WM, FL, and HAZ. A significant drop in absorbed energy values is present in the top and bottom parts of the X-welded joint cross section, corresponding to fill and cover passes, while the highest absorbed energy values are determined in the middle of welded joint cross-section, corresponding to the root passes.
- All welded joint regions are susceptible to exposure to PWHT thermal cycles, with hardness decreasing and temperatures increasing. This result is correlated with stress–strain behavior, where BM retains its properties, while HAZ exhibits substantial degradation of its properties.
- Metallographic examination of thermally exposed X-welded joint material does not show significant changes in the welded joint material (BM, HAZ, and WM). In general, dislocation density and precipitation result in change in such mechanical properties.
- Reductions in residual stresses are strongly dependent on PWHT temperatures. Measurements on S690QL1 steel X-welded joints show that 70% of relative stresses are eliminated at 400 °C, while only 40% are eliminated at 250 °C (Figure 24). It is clear that low temperature PWHT processes (<400 °C) can also yield good results if applied to S690QL1steel material. This method, however, needs to be experimentally proven through future research.
- In the authors' shared opinion, the optimal stress reduction temperature corresponds to PWHT Cycle C (max. 550 °C). This cycle achieves a significant 93% RS reduction (Figure 24), while mechanical properties are not significantly compromised and generally retain high values.

References

1. Miletić, I.; Ilić, A.; Nikolić, R.R.; Ulewicz, R.; Ivanović, L.; Sczygiol, N. Analysis of Selected Properties of Welded Joints of the HSLA Steels. *Materials* **2020**, *13*, 1301. [CrossRef] [PubMed]
2. Sisodia, R.P.S.; Gáspár, M. An Approach to Assessing S960QL Steel Welded Joints Using EBW and GMAW. *Metals* **2022**, *12*, 678. [CrossRef]
3. SSAB. *Welding Handbook: A Guide to Better Welding of Hardox and Strenx*, 2nd, ed.; SSAB: Oxelösund, Sweden, 2019.
4. Dillinger Hütte. *DILLIMAX Technical Information No.III/2007*; Dillinger Hütte GTS: Dillingen, Germany, 2007.
5. Tomerlin, D.; Kozak, D.; Damjanović, D.; Katinić, M. Structural life analysis method applied to hydraulic press welded frame construction. *Weld World* **2022**, *66*, 2595–2607. [CrossRef]
6. *Welding and Joining of Advanced High Strength Steels (AHSS)*, 1st ed.; Shome, M.; Tumuluru, M. (Eds.) Woodhead Publishing: Cambridge, UK, 2015.
7. Tamura, I.; Sekine, H.; Tanaka, T. *Thermomechanical Processing of High-Strength Low-Alloy Steels*; Butterworth-Heinemann: Oxford, UK, 1988.
8. Górka, J. Assessment of Steel Subjected to the Thermomechanical Control Process with Respect to Weldability. *Metals* **2018**, *8*, 169. [CrossRef]
9. Ilsenburger Grobblech GmbH Fine-Grain Structural Steels—MAXIL®690. Available online: https://www.ilsenburger-grobblech.de/fileadmin/footage/MEDIA/gesellschaften/ilg/dokumente/Werkstoffblaetter/Werkstoffblaetter_englisch/2022_Fine-Grain_Structural_Steels_MAXIL690.pdf (accessed on 8 February 2023).
10. SSAB Strenx 700 E/F General Product Description. Available online: https://www.ssab.com/en/products/brands/strenx/produ-cts/strenx-700-e-f (accessed on 8 February 2023).
11. Böhler Welding by Voestalpine Filler Metals Bestseller for Joining Applications. Available online: https://welding-expert.com/uploads/media/Weldingguide_ENGnew.pdf (accessed on 8 February 2023).
12. Mert, T.; Tümer, M.; Kerimak, Z.M. Investigations on Mechanical Strength and Microstructure of Multi-Pass Welded S690QL HSLA Steel Using MAG and FCAW. *Pract. Metallogr.* **2019**, *56*, 634–654. [CrossRef]
13. Cai, W.-Y.; Wang, Y.-B.; Li, G.-Q.; Stroetmann, R. Comparative study on strength of TMCP and QT high-strength steel butt-welded joints. *J. Constr. Steel Res.* **2022**, *197*, 107447. [CrossRef]
14. Macdonald, K.A. *Fracture and Fatigue of Welded Joints and Structures*; Woodhead Publishing Ltd.: Cambridge, UK, 2011.
15. Tall, L. Residual Stresses in Welded Plates—A Theoretical Study, No. 235 (64-1). In Proceedings of the Spring Meeting of the AWS in Dallas, Fritz Laboratory Reports. Dallas, TX, USA, September 1961; p. 1680.
16. Alipooramirabad, H.; Ghomashchi, R.; Paradowska, A.; Reid, M. Residual stress-microstructure-mechanical property interrelationships in multipass HSLA steel welds. *J. Mater. Process. Technol.* **2016**, *231*, 456–467. [CrossRef]
17. Bukovská, Š.; Moravec, J.; Solfronk, P.; Pekárek, M. Assessment of the Effect of Residual Stresses Arising in the HAZ of Welds on the Fatigue Life of S700MC Steel. *Metals* **2022**, *12*, 1890. [CrossRef]
18. ASM International. *ASM Handbook, Volume 4: Heat Treating*; ASM International: Materials Park, OH, USA, 1991; ISBN 978-1-62708-011-8.
19. Hrivnak, I. *Theory of Weldability of Metals and Alloys*; Elsevier Science Ltd.: Amsterdam, Netherlands, 1992; ISBN 0-444-98707-X.
20. Alipooramirabad, H.; Paradowska, A.; Reid, M.; Ghomashchi, R. Effects of PWHT on the Residual Stress and Microstructure of Bisalloy 80 Steel Welds. *Metals* **2022**, *12*, 1569. [CrossRef]
21. Zhao, M.S.; Chiew, S.P.; Lee, C.K. Post weld heat treatment for high strength steel welded connections. *J. Constr. Steel Res.* **2016**, *122*, 167–177. [CrossRef]
22. Kik, T.; Moravec, J.; Švec, M. Experiments and Numerical Simulations of the Annealing Temperature Influence on the Residual Stresses Level in S700MC Steel Welded Elements. *Materials* **2020**, *13*, 5289. [CrossRef] [PubMed]
23. Wang, X.; Wang, D.; Dai, L.; Deng, C.; Li, C.; Wang, Y.; Shen, K. Effect of Post-Weld Heat Treatment on Microstructure and Fracture Toughness of X80 Pipeline Steel Welded Joint. *Materials* **2022**, *15*, 6646. [CrossRef] [PubMed]
24. Ono, Y.; Yıldırım, H.C.; Kinoshita, K.; Nussbaumer, A. Damage-Based Assessment of the Fatigue Crack Initiation Site in High-Strength Steel Welded Joints Treated by HFMI. *Metals* **2022**, *12*, 145. [CrossRef]
25. Samardžić, I.; Vuherer, T.; Marić, D.; Konjatić, P. Influence of vibrations on residual stresses distribution in welded joints. *Metalurgija* **2015**, *54*, 527–530.
26. de Moraes, A.G.; Clarke, T.G.R.; Diehl, I.L. Quantification of CTOD fracture toughness in welded joints to evaluate the efficacy of vibration stress relief compared to thermal stress relief. *Mater. Res.* **2020**, *23*, e20200157. [CrossRef]
27. Glaser, B.; Predan, J.; Kozak, D.; Gubeljak, N. Comparison between Stereo Optical Strain Measurements and Finite Element Results in Stress Concentration Zones. *Tech. Gaz.* **2019**, *26*, 1346–1352.
28. Saber, M. Bending Test and Simulation of Welded Galvanized Steel Pipes. *Tech. Gaz.* **2021**, *28*, 509–514.
29. Suominen, L.; Khurshid, M.; Parantainen, J. Residual stresses in welded components following post-weld treatment methods. *Procedia Eng.* **2013**, *66*, 181–191. [CrossRef]
30. Lu, W.; Sun, J.; Su, H.; Gao, C.; Zhang, X. Experimental Research of Welding Residual Stress of Butt Welded Joint of Thick Steel Plate. *Metals* **2023**, *13*, 120. [CrossRef]
31. Mateša, B.; Kožuh, Z.; Dunđer, M.; Samardžić, I. Determination of Clad Plates Residual Stresses by X-ray Diffraction Method. *Tech. Gaz.* **2015**, *22*, 1533–1538.

32. Starčevič, L.; Gubeljak, N.; Predan, J. The Numerical Modelling Approach with a Random Distribution of Mechanical Properties for a Mismatched Weld. *Materials* **2021**, *14*, 5896. [CrossRef] [PubMed]
33. Hertelé, S.; Bally, J.; Gubeljak, N.; Stefane, P.; Verleysen, P.; De Waele, W. Characterization of Heterogeneous Arc Welds through Miniature Tensile Testing and Vickers Hardness Mapping. *Mater. Tehnol.* **2016**, *50*, 571–574. [CrossRef]
34. Clyne, T.W.; Campbell, J.E.; Burley, M.; Dean, J. Profilometry-Based Inverse Finite Element Method Indentation Plastometry. *Adv. Eng. Mater.* **2021**, *23*, 2100437. [CrossRef]
35. Gu, W.; Campbell, J.; Tang, Y.; Safaie, H.; Johnston, R.; Gu, Y.; Pleydell-Pearce, C.; Burley, M.; Dean, J.; Clyne, T.W. Indentation Plastometry of Welds. *Adv. Eng. Mater.* **2022**, *24*, 2101645. [CrossRef]